The Abdus Salam
International Centre for Theoretical Physics

United Nations
Educational, Scientific and
Cultural Organization

IAEA

310/1828 310/14

Workshop on Biomedical Applications of High Energy Ion Beams

Co-sponsored by: ICGEB and University of Surrey

12-16 February 2007

Venue:
Adriatico Guest House Giambiagi Lecture Hall
ICTP, Trieste, Italy

Bio-medical Imaging with Synchrotron Radiation

Giuliana TROMBA
Elettra Sincrotrone Trieste, Italy

Bio-medical imaging with Synchrotron Radiation: the experience at the SYRMEP beamline

Giuliana Tromba
Sincrotrone Trieste

Outline

- **Introduction to the ELETTRA laboratory**
- **New phase-sensitive SR-based techniques**
- **Recent results at the SYRMEP beamline**
- **The project for clinical mammography**

ELETTRA light source

ELETTRA layout

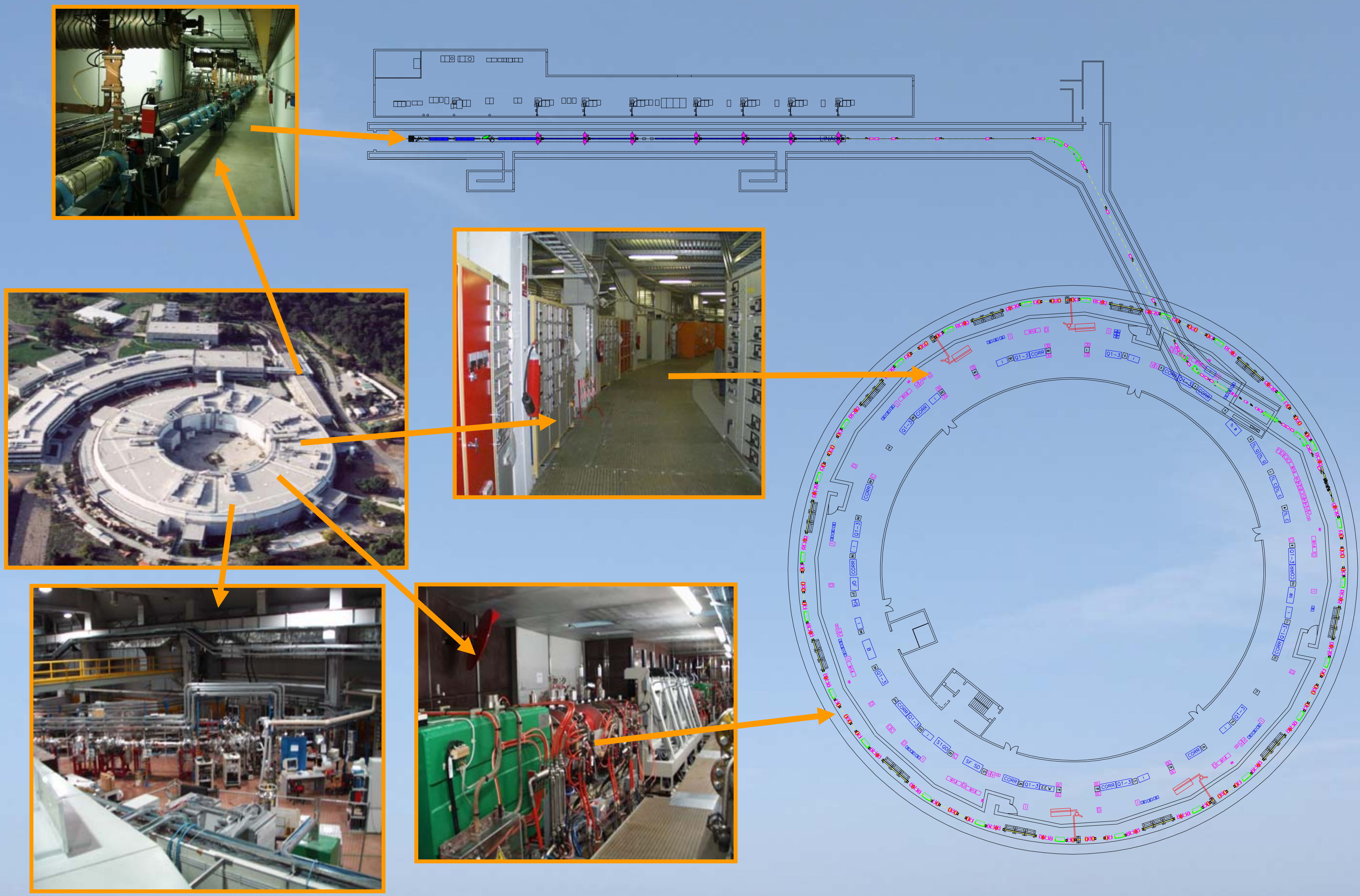

Elettra Achromat

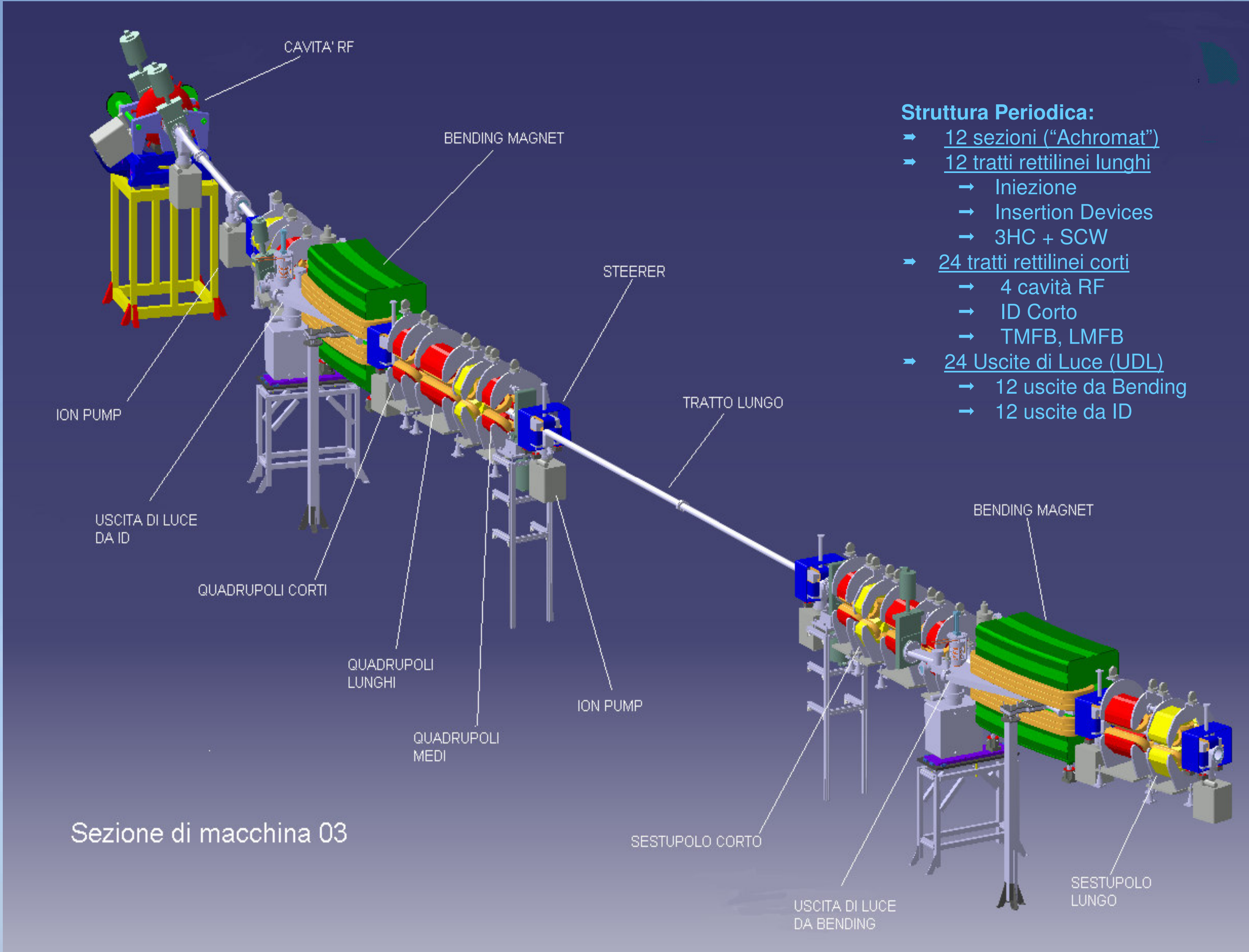

Struttura Periodica:

- 12 sezioni ("Achromat")
- 12 tratti rettilinei lunghi
  - Iniezione
  - Insertion Devices
  - 3HC + SCW
- 24 tratti rettilinei corti
  - 4 cavità RF
  - ID Corto
  - TMFB, LMFB
- 24 Uscite di Luce (UDL)
  - 12 uscite da Bending
  - 12 uscite da ID

The magnets

Dipole
Quadrupole (red)
Sextupole
Corrector

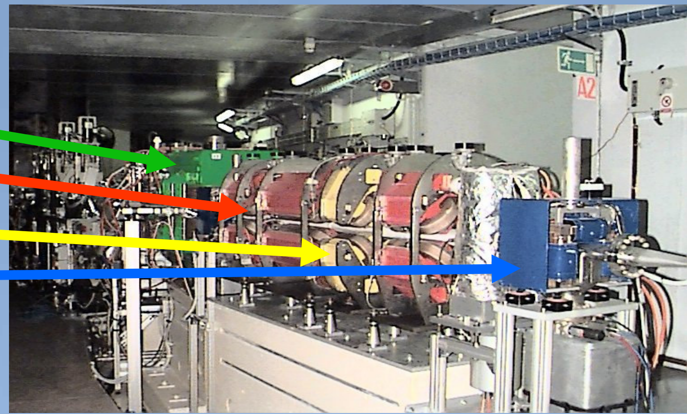

Insertion Devices (ID's)

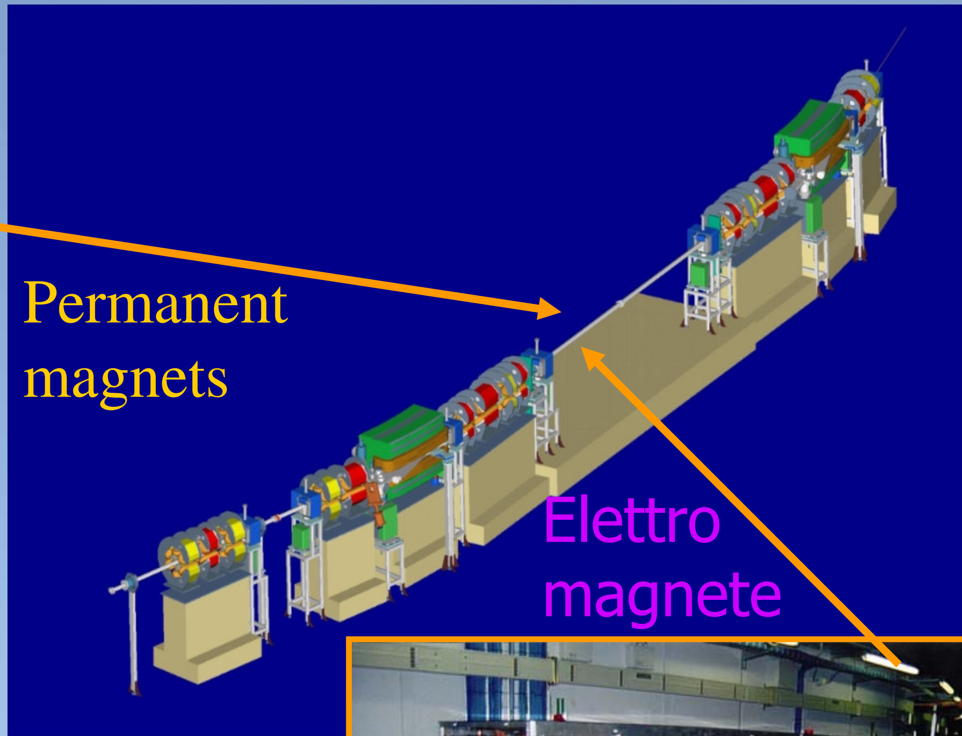

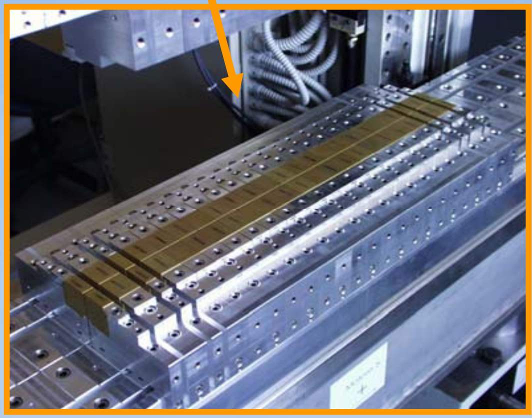

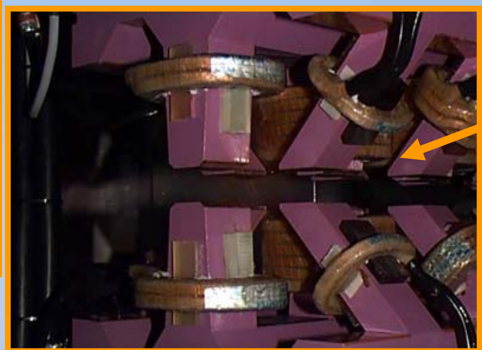

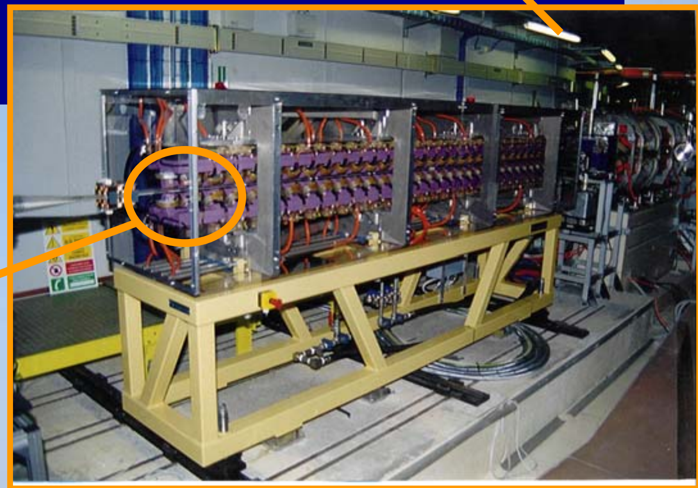

The beamlines

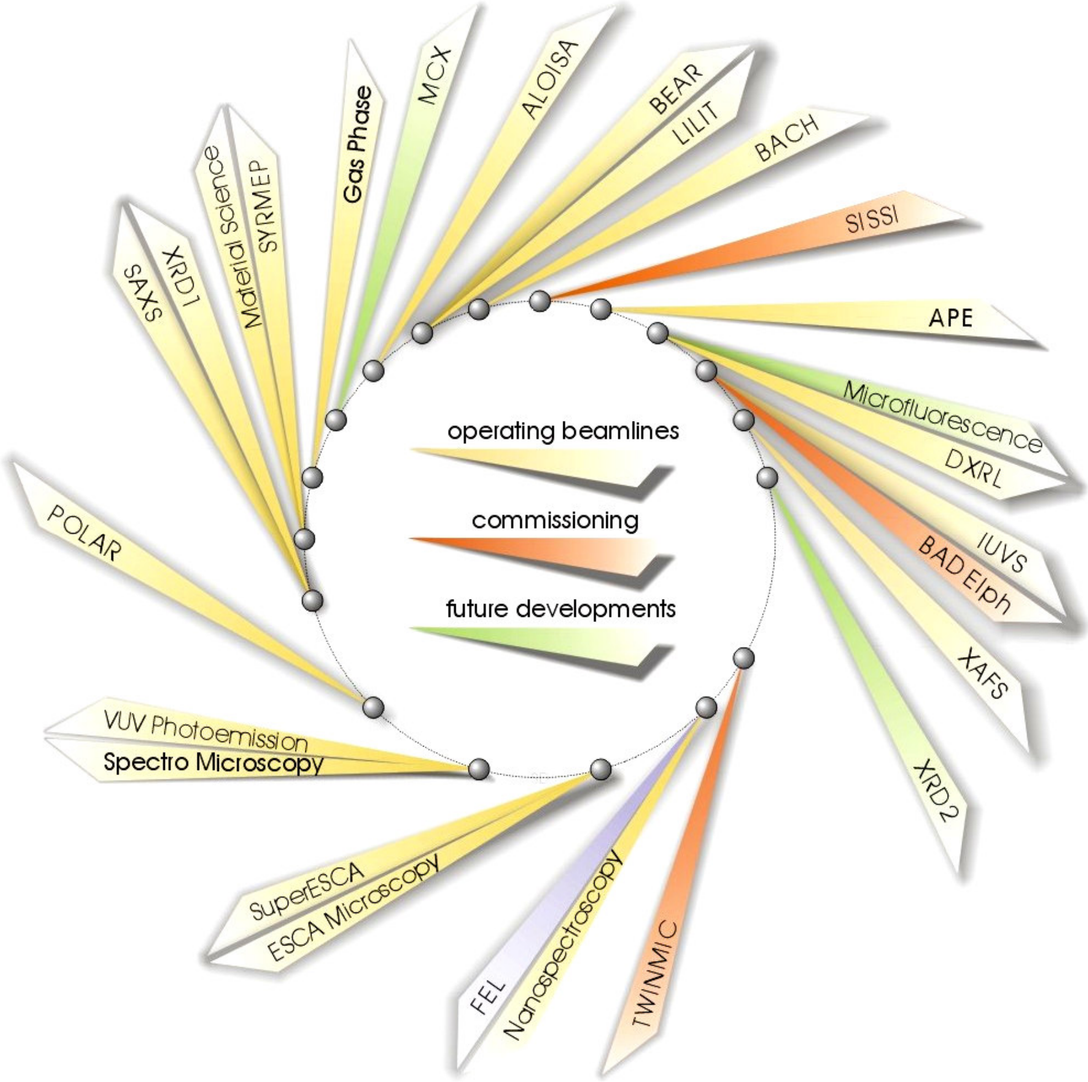

Exit	Beamline	Source
1.1L	TWINMIC	short id
1.2L	Nanospectroscopy	id
1.2R	FEL (Free Electron Laser)	-
2.2L	ESCA Microscopy	id
2.2R	SuperESCA	id
3.2L	Spectromicroscopy	id
3.2R	VUV Photoemission	id
4.2	POLAR (Circular Polarized Light)	id
5.2L	SAXS (Small Angle X-ray Scattering)	id
5.2R	XRD1 (X-ray Diffraction)	id
6.1L	MSB (Material Science Beamline)	bm
6.1R	SYRMEP (Synchrotron Radiation for Medical Physics)	bm
6.2R	Gas Phase	id
7.1	MCX (Powder Diffraction Beamline)	bm
7.2	ALOISA (Advanced Line for Overlayer, Interface and Surface Analysis)	id
8.1L	BEAR (Bending Magnet for Emission Absorption and Reflectivity)	bm
8.1R	LILIT (Lab of Interdisciplinary LIThography)	id
8.2	BACH (Beamline for Advanced DiCHroism)	id
9.1	SISSI (Source for Imaging and Spectroscopic Studies in the Infrared)	bm
9.2	APE (Advanced Photoelectric-effect Experiments)	id
10.1L	X-ray Microfluorescence	bm
10.1R	DXRL (Deep-etch Lithography)	bm
10.2L	IUVS (Inelastic Ultra Violet Scattering)	id
10.2R	BAD Elph	id
11.1R	XAFS (X-ray Absorption Fine Structure)	bm
11.2	XRD2 (X-ray Diffraction)	id

Main advantages in the use of SR for bio-medical imaging

- Monochromaticity -> no beam hardening
  k-edge imaging
  quantitative evaluations
  optimization of X-ray energy with sample characteristics (dose reduction)
- Collimation -> parallel beams, scatter reduction
- Spatial coherence -> application of *phase sensitive* techniques
- High intensity -> reduction of exposure time

Phase-sensitive imaging techniques

Conventional radiology relies on X-ray absorption as the unique source of contrast and is based exclusively on the detection of amplitude variation of the transmitted X-rays.
Main limitation $\longrightarrow$ poor contrast for samples with low-Z composition.

Phase sensitive imaging techniques are based on the observation of the *phase shifts* produced by the object on the incoming wave.

Refractive index: $n = 1 - \delta + i\,\beta$
β = absorption term; δ = phase shift term
$\beta \sim 10^{-10}$; $\delta \sim 10^{-6}$ in soft tissue @ 17 keV
$\delta \propto \lambda^2$, $\beta \propto \lambda^3$
Absorption radiology -> contrast generated by differences in the x-ray absorption ($\beta\,\Delta z$)
Phase Radiology –> contrast generated by phase shifts x-ray absorption ($\delta\,\Delta z$)
($\delta \gg \beta$ –> phase contrast >> absorption contrast

PHase-Contrast radiography (PHC)

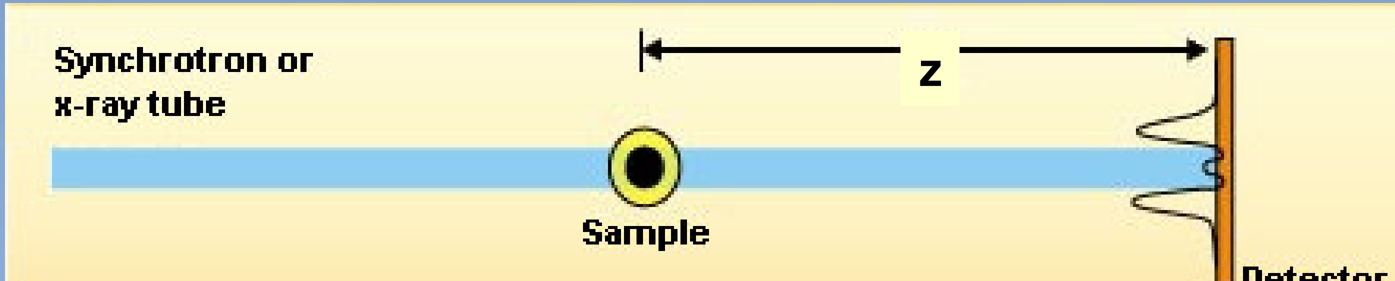

R.Fitzgerard, Physics Today, July 2000

- Similar to technique for in-line holography by D.Gabor (1948), first implementation with a conventional source was by Davis et al. (Nature 373, 1995) and with SR by A.Snigirev et al. *(Rev.Sci.Instrum., 66, 1995).* F.Arfelli et al. (Phys.Med.Biol. 43, 1998) implemented it for medical imaging.
- The technique exploits the high spatial coherence of the X-ray source.
- z =0 -> absorption image
- For z > 0 -> interference between diffracted and un-diffracted wave produces edge and contrast enhancement. A variation of δ is detected
- Measure of $\nabla^2\Phi(x,y)$

Regimes

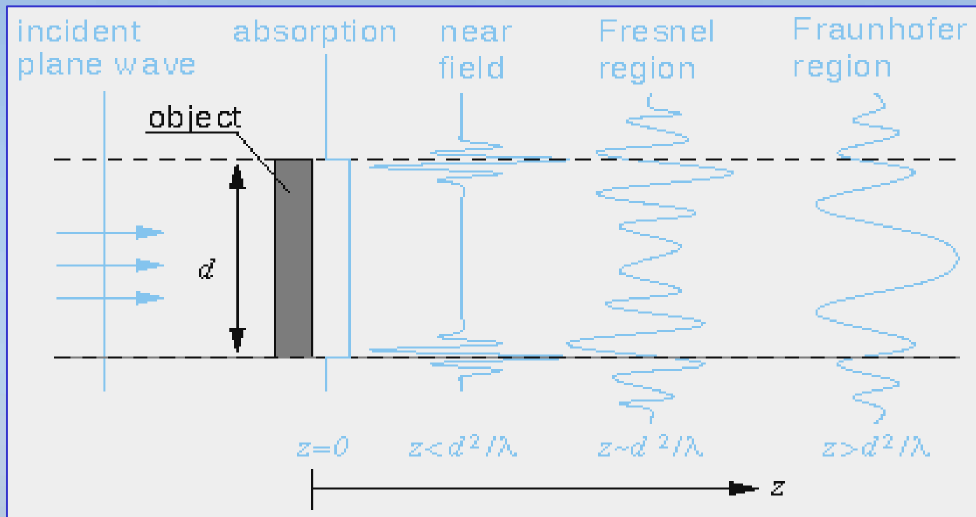

Simulated PHC patterns for a 100 mm nylon wire

Influence of:

- Source dimension
- Sample-to-det. distance
- Detector resolution

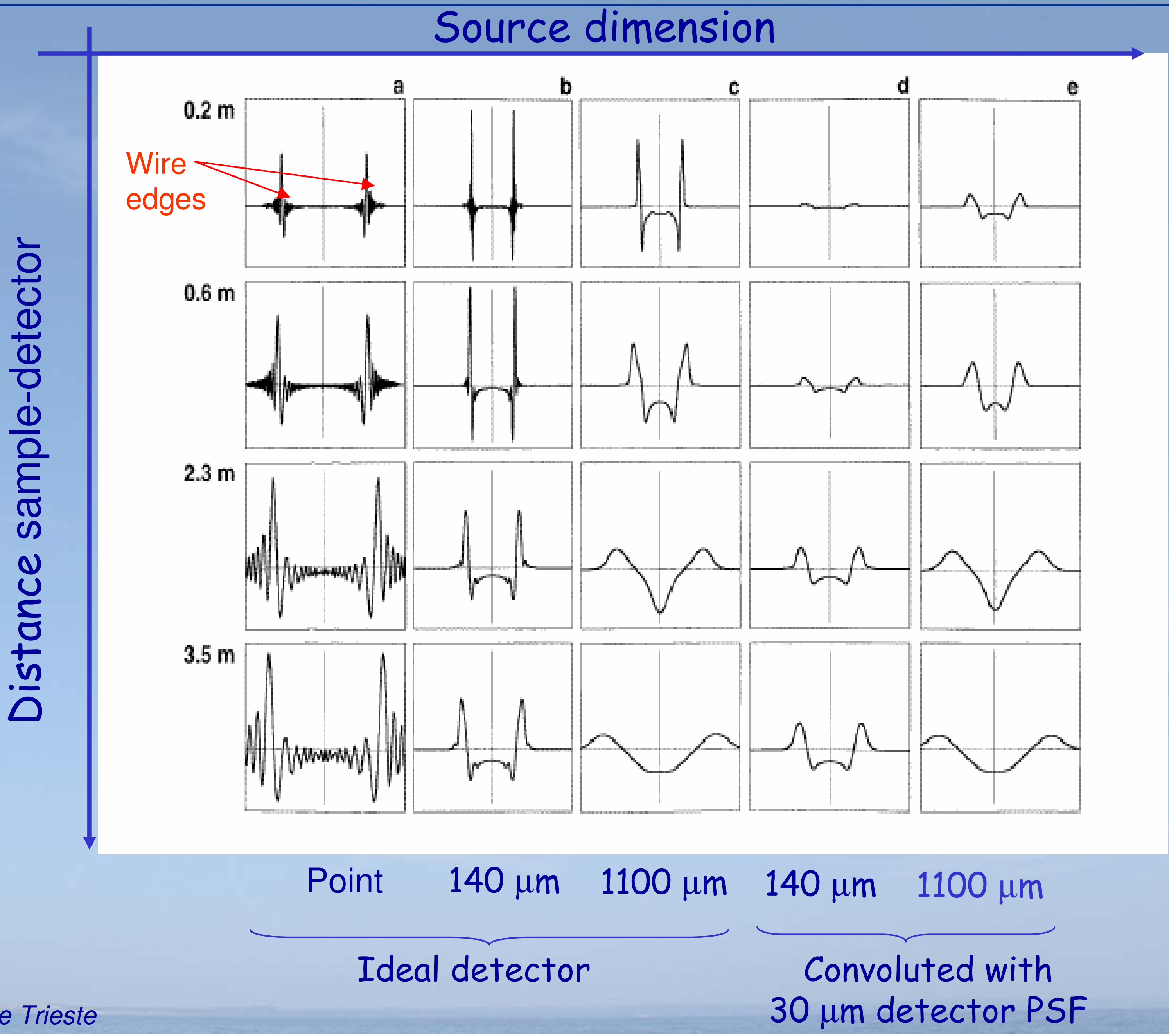

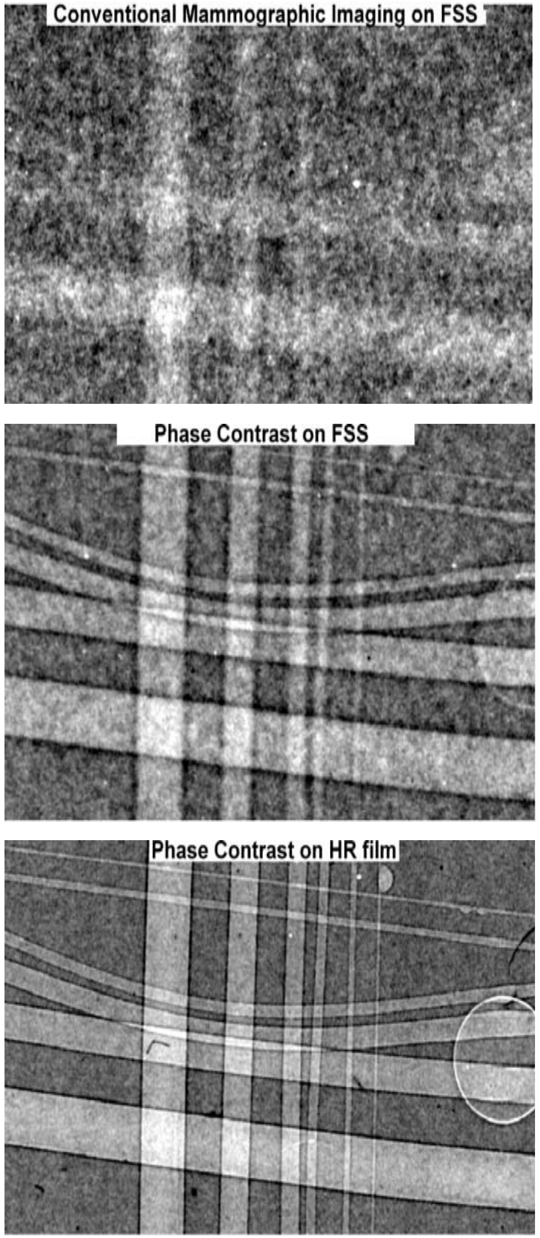

Real images
of nylon wires

Images of a Mimosa flower

10 keV

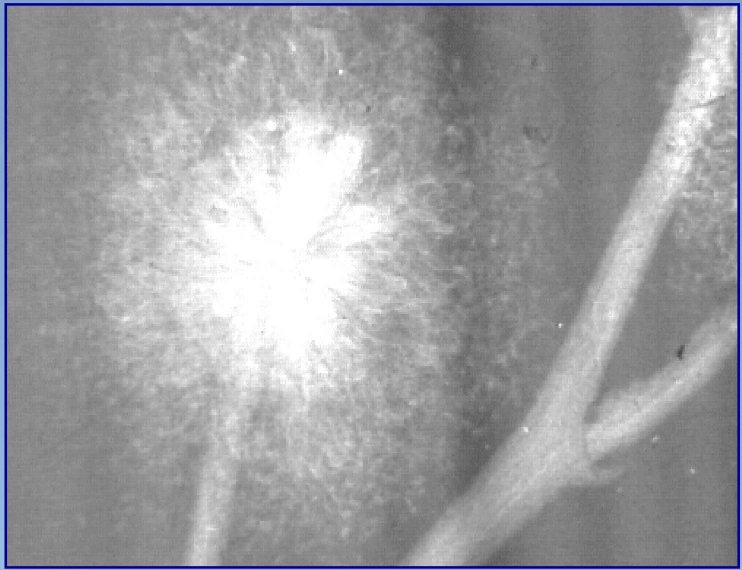

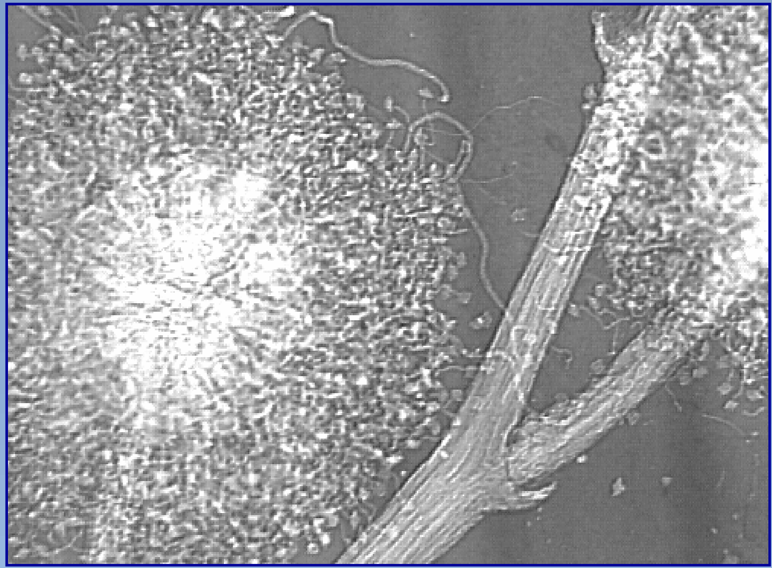

Absorption **Phase-contrast**

25 keV

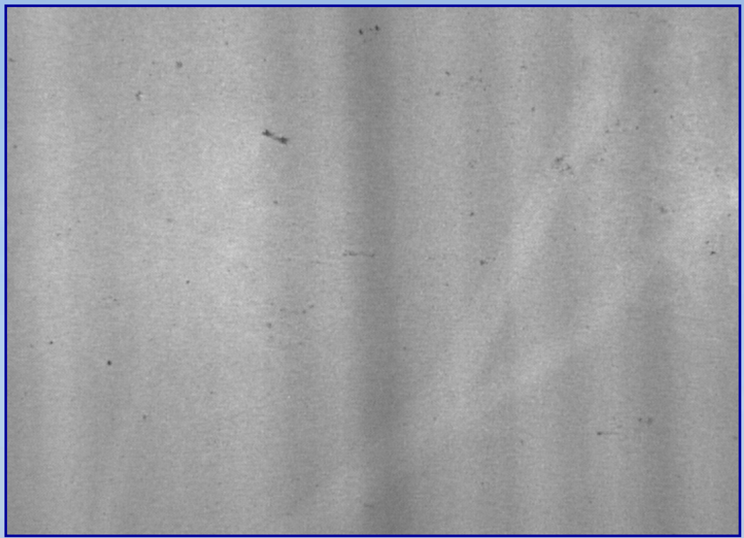

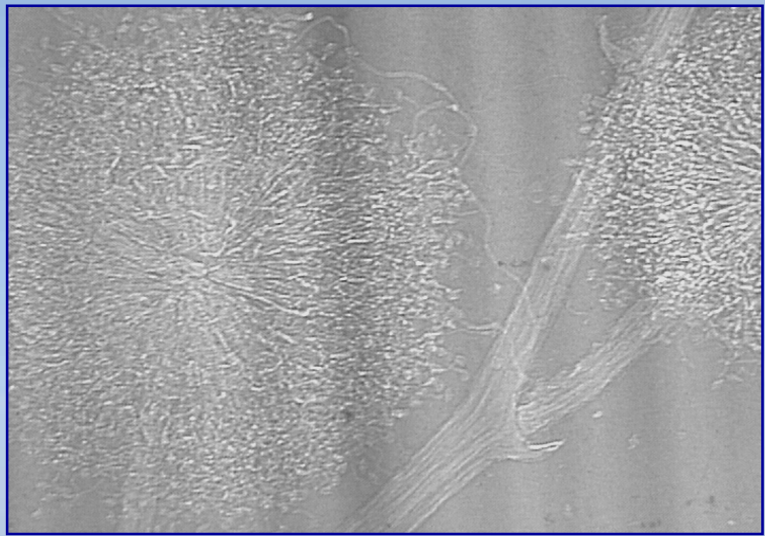

Diffraction Enhanced Imaging (DEI)

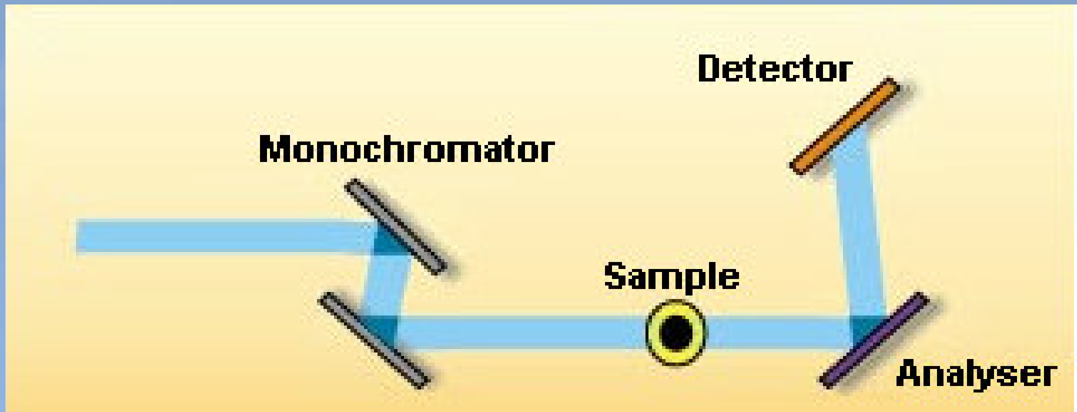

R.Fitzgerard, Physics Today, July 2000

- The technique was first explored by K.M. Podurets et al. (Sov. Phys. Tech. Phys. 34(6), June 1989) and by Ingal et al. (App. Phys. 28, 1995) with different names as “refraction-contrast radiography”, “phase dispertion introscopy”. First physics interpretation by D.Chapman et al., Phys.Med.Biol. 42, 1997.
- A perfect crystal is used as an angular filter to select angular emission of X-rays. The filtering function is the rocking curve (FWHM: 1-20 μrad)
- Analyzer and monochromator aligned -> X-ray scattered by more than some tens μrad are rejected
- Small misalignements -> investigation of phase shift effects (refraction angle is roughly proportional to the gradient of δ)
- With greater misalignements the primary beam is almost totally rejected and pure refraction images are obtained
- $\nabla\Phi(x,y)$

DEI image manipulation

I_L

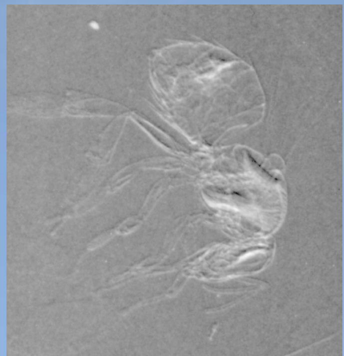

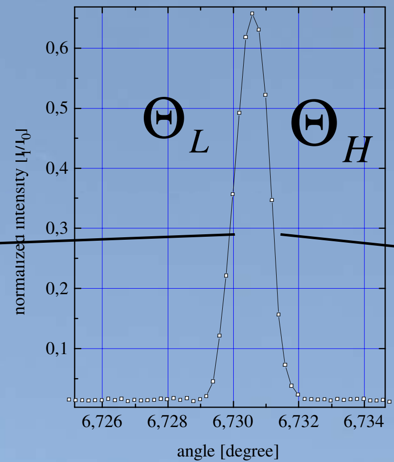

I_H

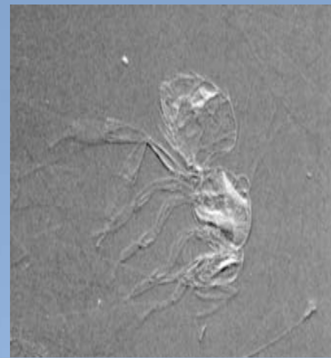

$$I_L = I_R\left(R(\Theta_L) + \frac{\partial R}{\partial \Theta}(\Theta_L)\Delta\Theta_z\right)$$

$$I_H = I_R\left(R(\Theta_H) + \frac{\partial R}{\partial \Theta}(\Theta_H)\Delta\Theta_z\right)$$

Θ_Z = refraction Image

I_R = apparent absorption image (absorption+extinction)

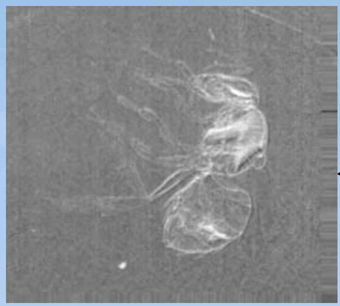

Apparent Absorption Image

$$I_R = \frac{I_L \cdot \left.\frac{dR}{d\Theta}\right|_{\Theta_H} - I_H \cdot \left.\frac{dR}{d\Theta}\right|_{\Theta_L}}{R(\Theta_L)\cdot \left.\frac{dR}{d\Theta}\right|_{\Theta_H} - R(\Theta_H)\cdot \left.\frac{dR}{d\Theta}\right|_{\Theta_L}}$$

$$\Theta_Z = \frac{I_H \cdot R(\Theta_L) - I_L \cdot R(\Theta_H)}{I_L \cdot \left.\frac{dR}{d\Theta}\right|_{\Theta_H} - I_H \cdot \left.\frac{dR}{d\Theta}\right|_{\Theta_L}}$$

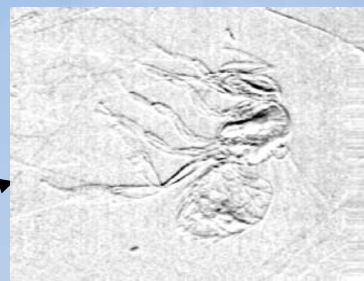

Refraction Image

Ref: Chapman et al, Phys.Med.Biol, 42,1997

SYRMEP layout for PHC imaging

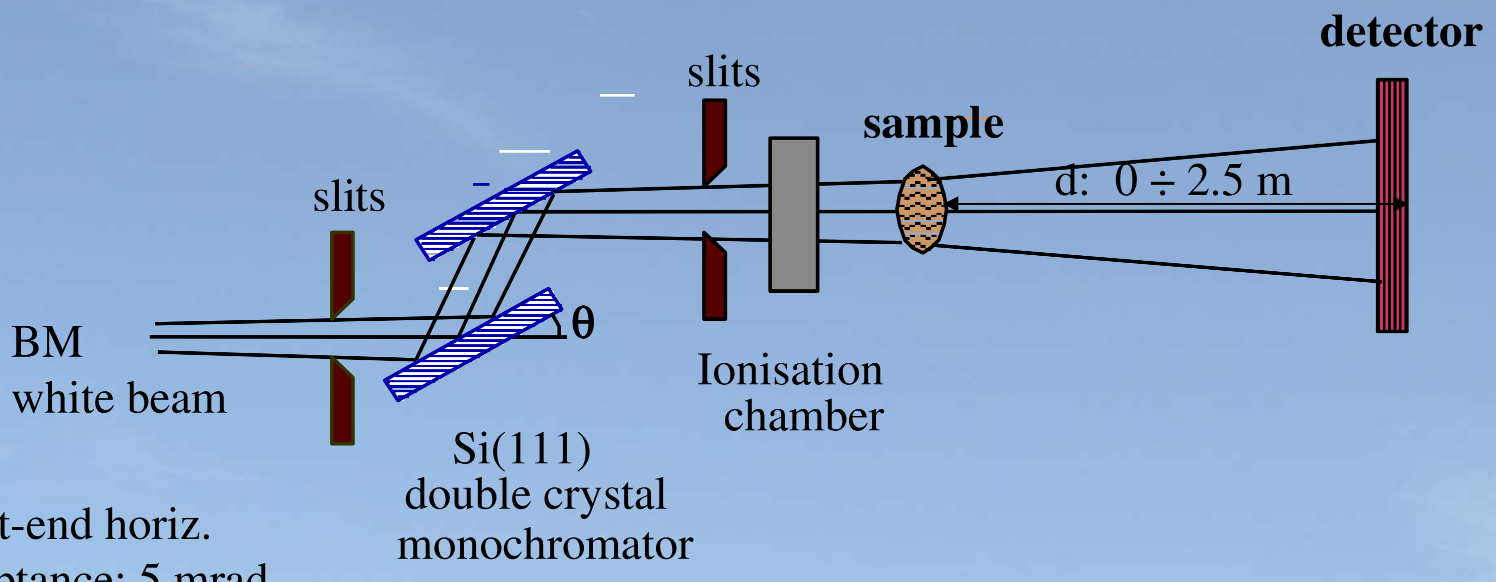

Front-end horiz.
acceptance: 5 mrad

SYRMEP beamline setup for DEI

Sources of contrast: absorption, extinction and refraction

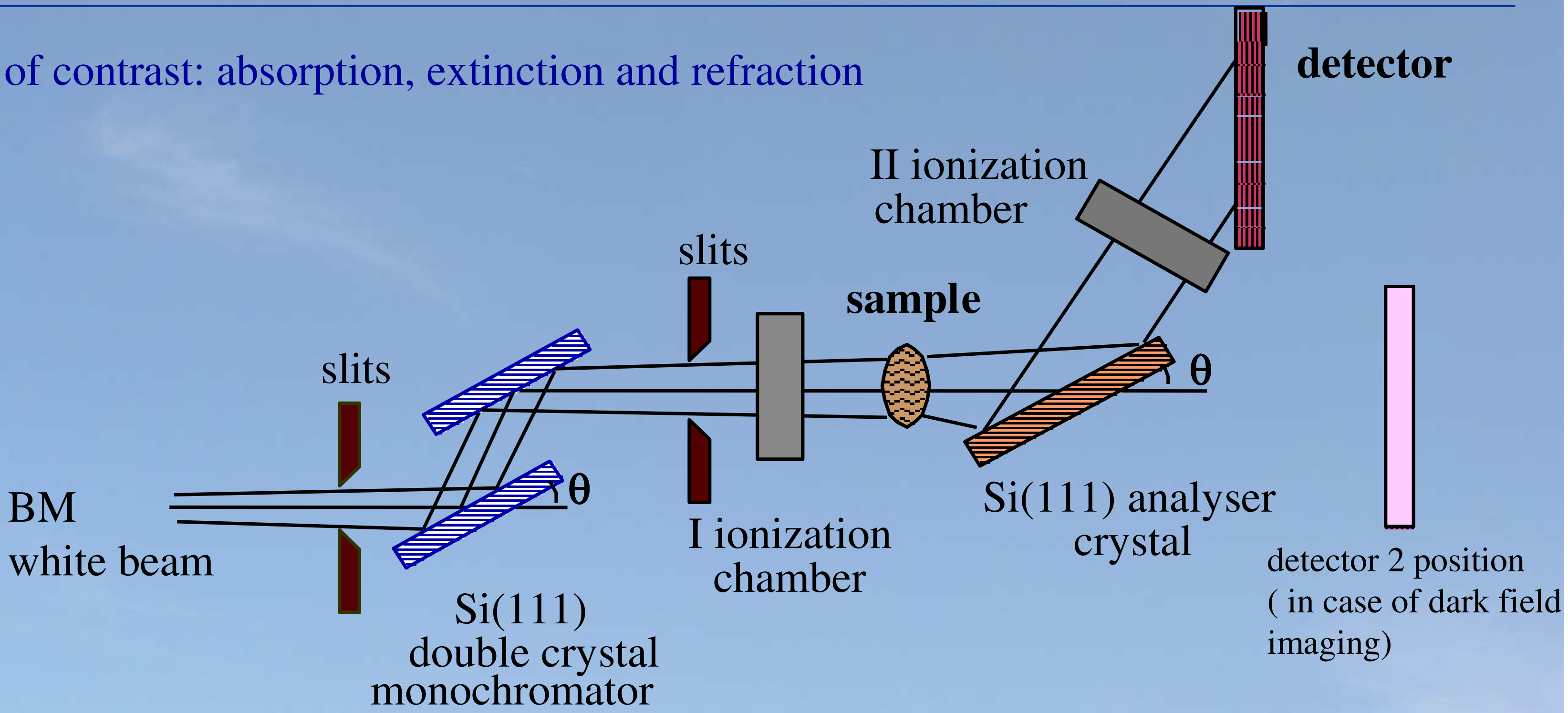

Refractive index $n = 1 - \delta + i\beta$

Variation of δ in the sample => Photons are refracted at μrad angles

- The analyzer crystal acts as a angular filter: filtering function is the rocking curve (FWHM: 1-20 μrad)
- Photons deviated outside the rocking curve width are not detected
- Photons deviated within the rocking curve width are diffracted towards the detector (probability modulated by the rocking curve)

Two ionization chambers allow to set the analyzer crystal on a certain position of the rocking curve

The SYRMEP beamline

Source Characteristics

- Source size ≅ 100 µm x 1100 µm
- Source-to-sample distance ≅ 23 m
- Sample-to-detector distance d: 0 ÷ 2.5 m
- Energy range: 8 ÷ 35 keV, Bandwidth $\Delta E/E \cong 10^{-3}$
- Typical fluxes at 15 keV ≅ $2 * 10^8$ phot./mm^2 s (@ 2 GeV, 300 mA)
  $7 * 10^8$ phot./mm^2 s (@ 2.4 GeV, 180 mA)
- Transverse coherence length at 15 keV ($L_c = \lambda L / 2^*\sigma$) ≅ 10 µm

Detectors

- High Resolution films (1 µm resolution)
- Medical screen-film systems (≅ 35 µm resolution)
- CCD (2048*2048 pixels) with 2 configurations:
  - pixel size: 14 µm, 1:1 optical fiber taper, field of view: 28.67x28.67 mm^2
  - pixel size: about 5 µm, with 11:40 magnifying optics, field of view of about 8mm^2.
- CCD (4008*2672 pixels), pixel size: 4.5 µm, 1:2 magn. optics, field of view: 18.04 x 12.02 mm^2
- Imaging Plate (IP reader FLA 7000 -25 µm resolution)

An example of image manipulation with DEI

Apparent absorption

Refraction image

DEI – images at two positions of the rocking curve

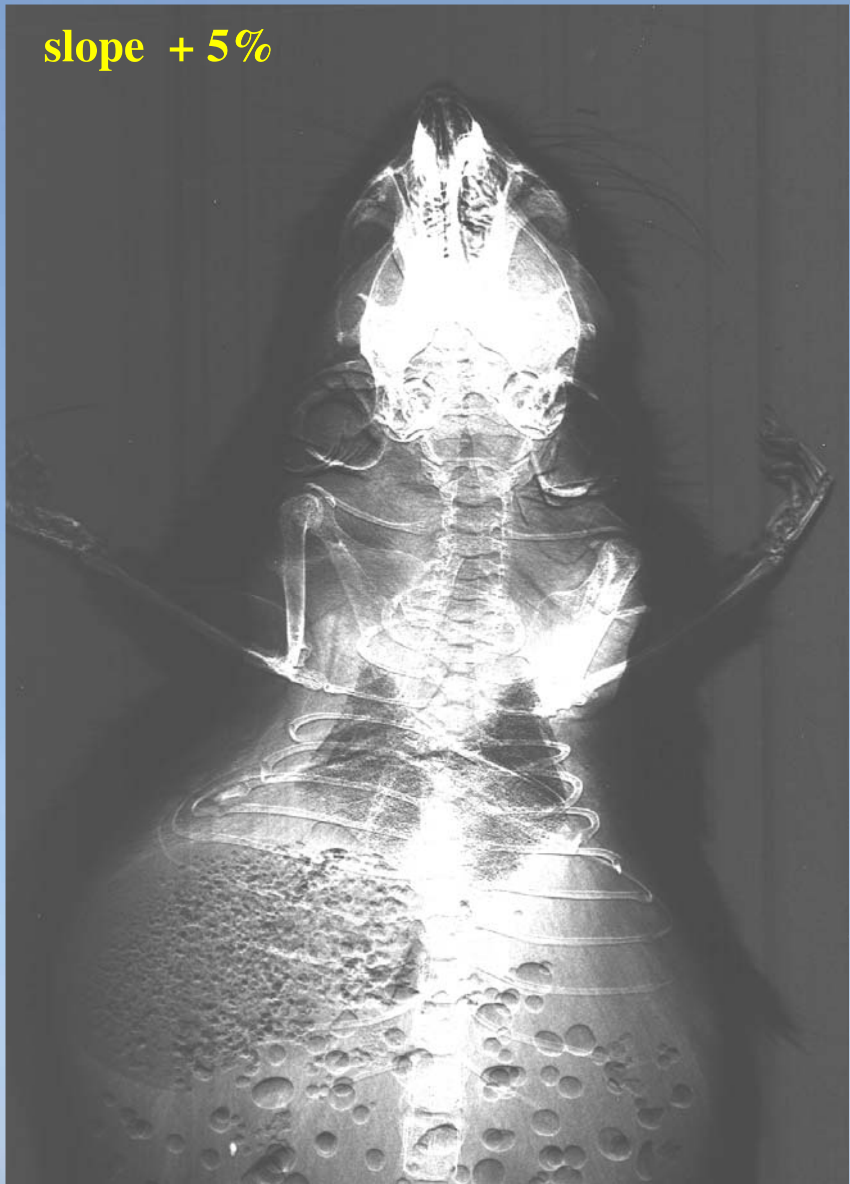

Recent results at the SYRMEP beamline

- Imaging of soft tissues and mammography (PHC) -> clinical trial with patient (SYRMA project)
- Imaging of brain tumors in rats
- Study of joints and cartilages (DEI)
- Imaging of lungs (DEI)
- Trabecular bone architecture (absorption tomo)
- Study of dental implants (absorption tomo)

Breast imaging

- Breast cancer is the most common cancer amongst women (incidence: 8%)
- The success of treatment depends on early detection (asynthomatic women)
- Main method for detecting early breast -> **X-ray mammography**
- Screening programs for large population area above 50 years old
- Sensitivity of conventional mammography: 85-90%, Specificity: 90%
- False positive/true positive ≈ 5 -10%
- High number of doubtful cases makes frequent the need of biopsies
- Conventional mammography is **not enough effective** for dense breasts

Radiographs of breasts with increasing density: mainly adipose breast (left) up to high fibro-glandularity breast (right)

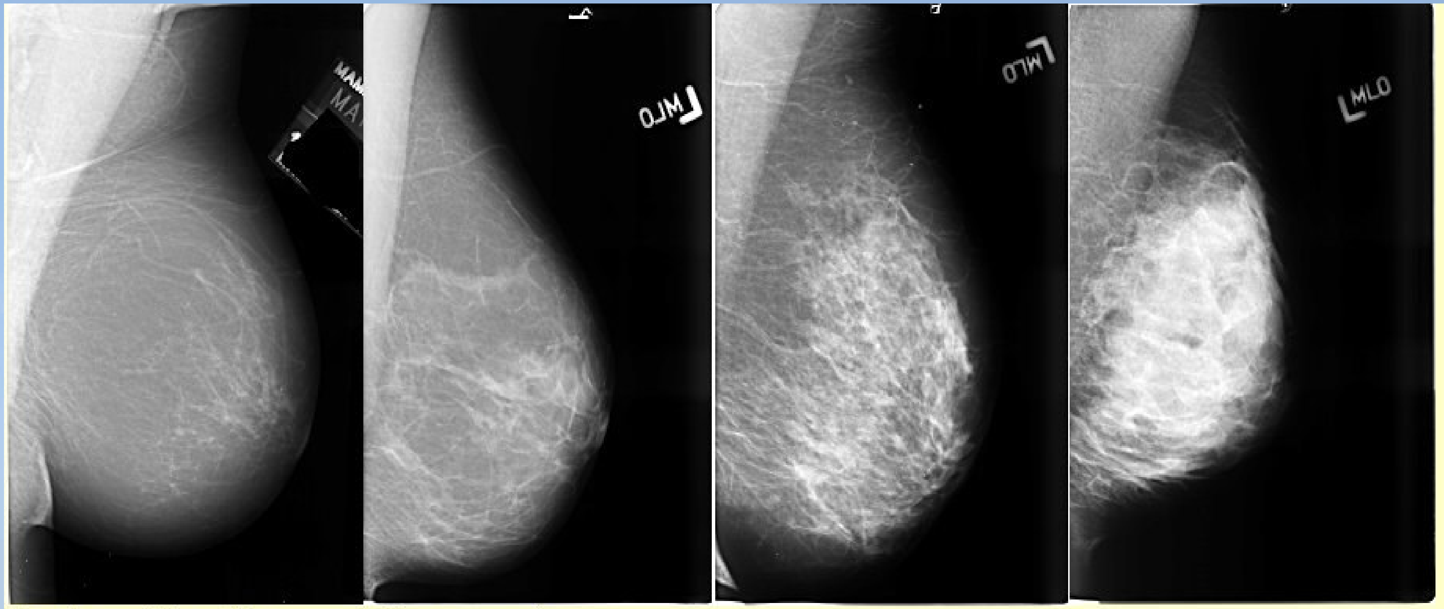

Breast composition and its mammographic appearance.[1]

PHC application to mammography: Human tissue sample

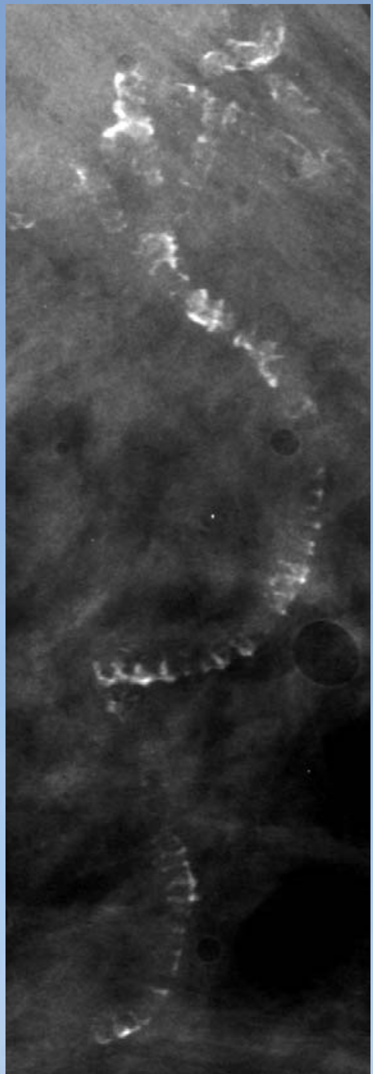

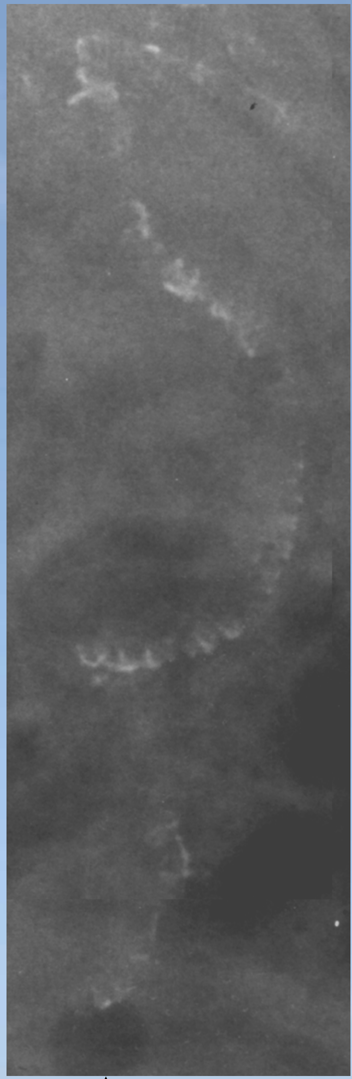

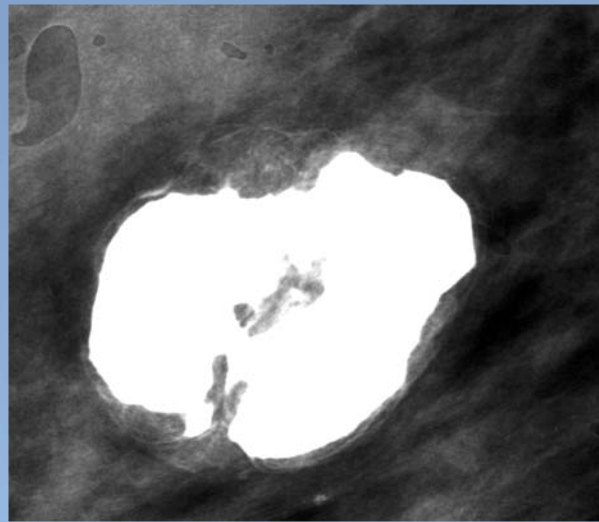

SR

E = 17 keV

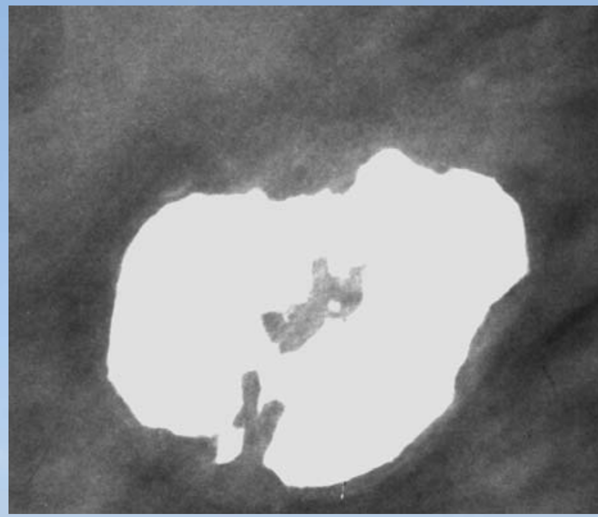

Thickness = 4 cm
MGD = 1.5 mGy

E = 17 keV

SR

Conventional X-ray generator

30 kVp, 50 mAs

The SYRMA project
(**SY**nchrotron **R**adiation for **Ma**mmography)

Agreement among the Public Hospital of Trieste, the University of Trieste and Elettra

Aim -> *In vivo* mammographic studies on limited number of cases selected by the Radiologist.

Target-> Patients with dense breasts,
conventional radiographs with uncertain diagnosis.

Set-ups-> I phase: PHC planar radiography with conventional screen-film system,
II phase: use of digital detectors,
III phase: application of tomography and tomosynthesis.

Clinical trial started on March 13, 2006.

Patients' selection

The patient recruitment is performed on the basis of the BI-RADS classes of the American College of Radiology (recognized by the European Guidelines for breast screening). A patient is a candidate suited to SR:

- if conventional mammography, for a symptomatic patient, shows a dense disomogeneus breast and Ultra-Sound (US) does not solve the problem (class R1);
- if mammography shows an asymmetry of the two breasts not understood by US (class R3);
- if both mammography and US detect doubtful lesions (class R3 and R4).

Methods used for comparing SR vs. conventional images

Better lesions characterization

Enhanced visibility of microcalcifications

Detectability of new lesions.

The SYRMA beamline

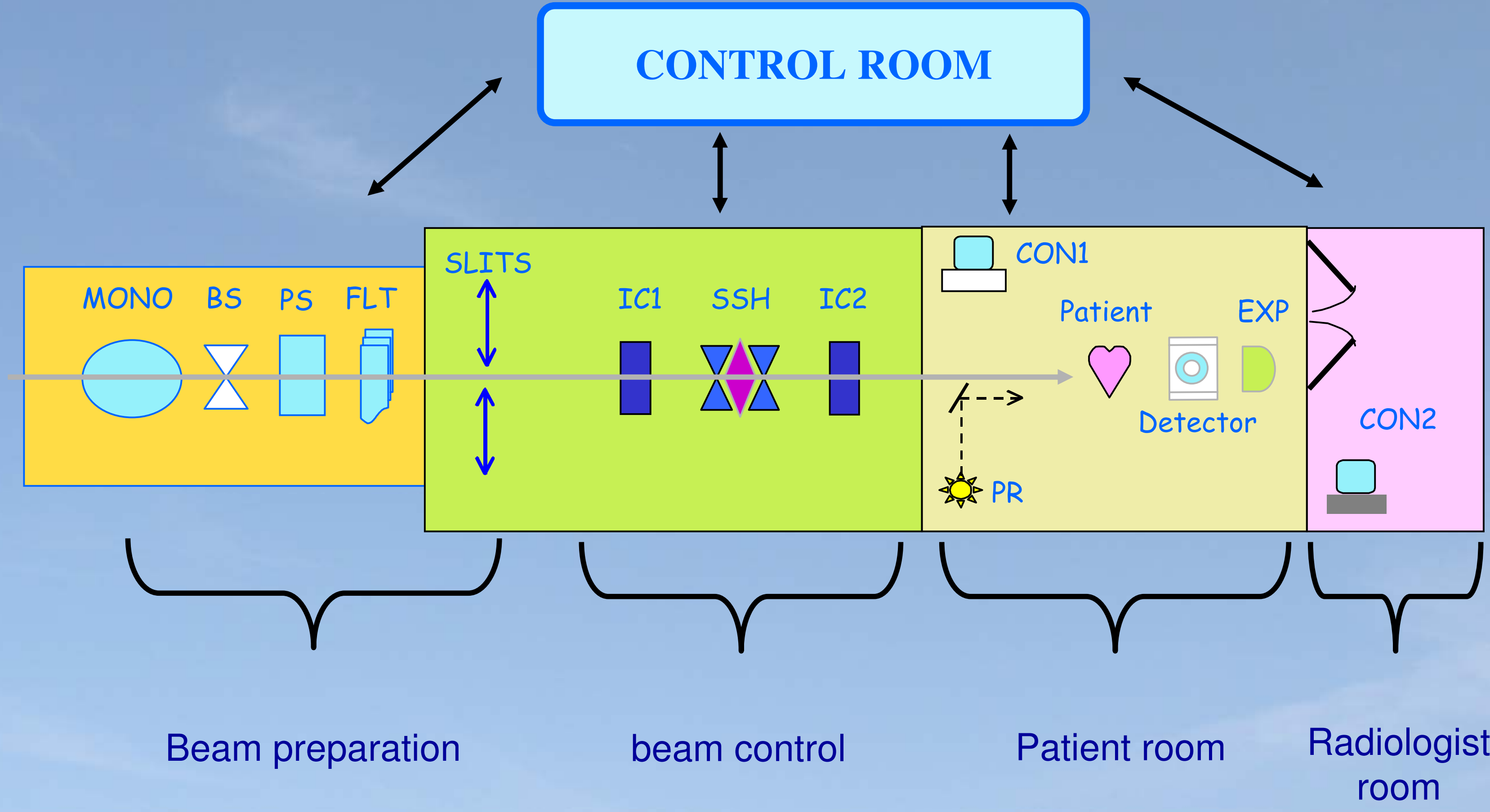

Safety systems:

- Beamline access control system (for personnel)
- Dose control system (for patient)

Dose monitoring and shutters

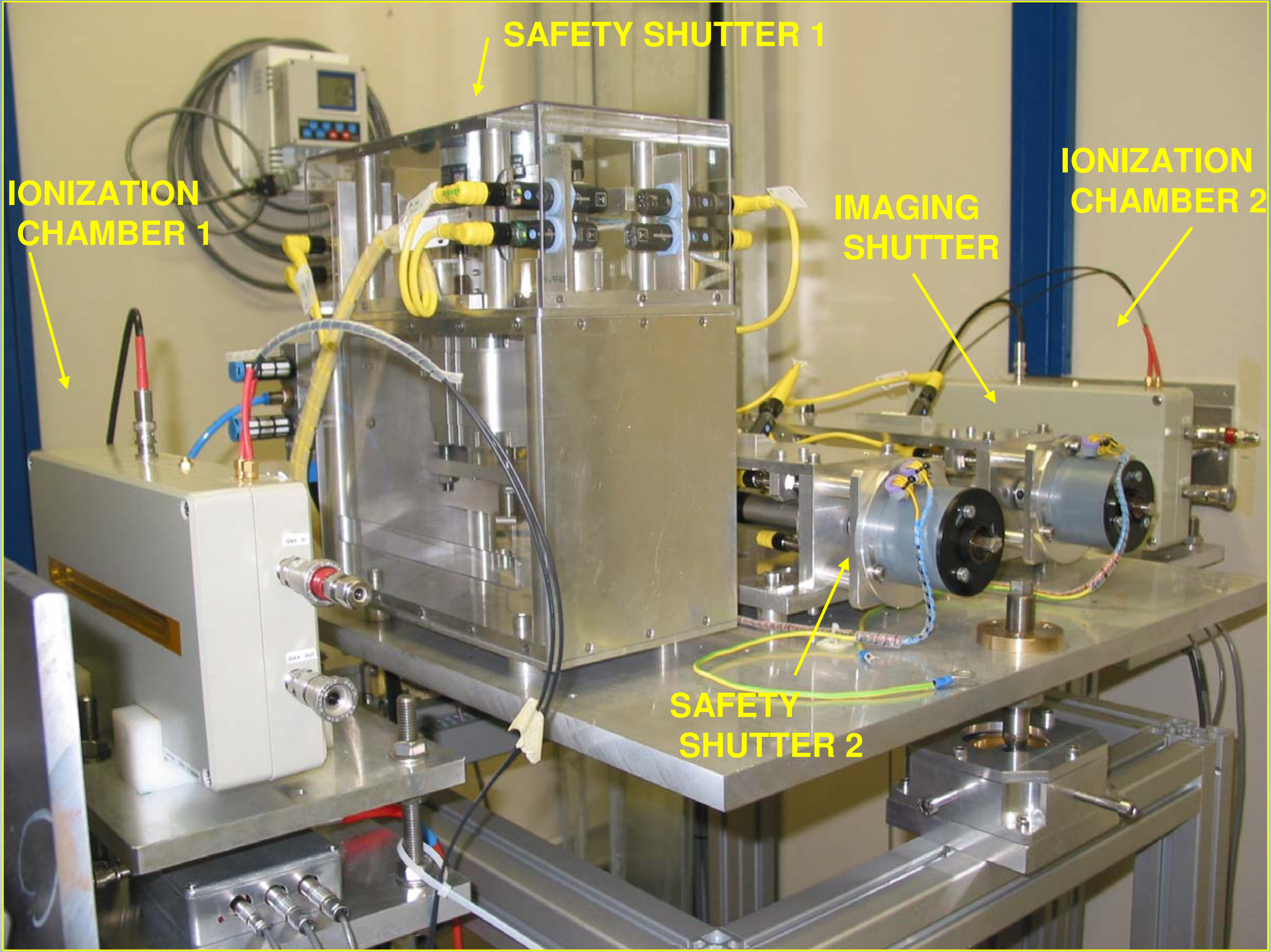

Radiologist room

Patient positioning

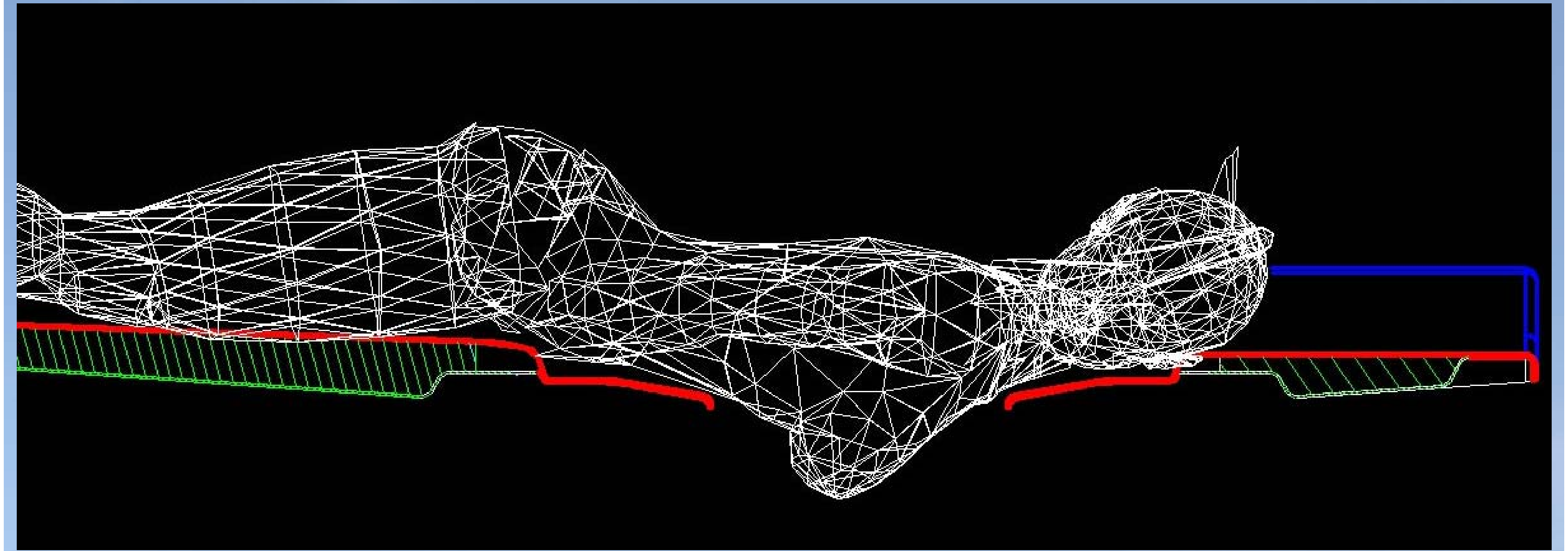

Patient room

Patient support

Compression system

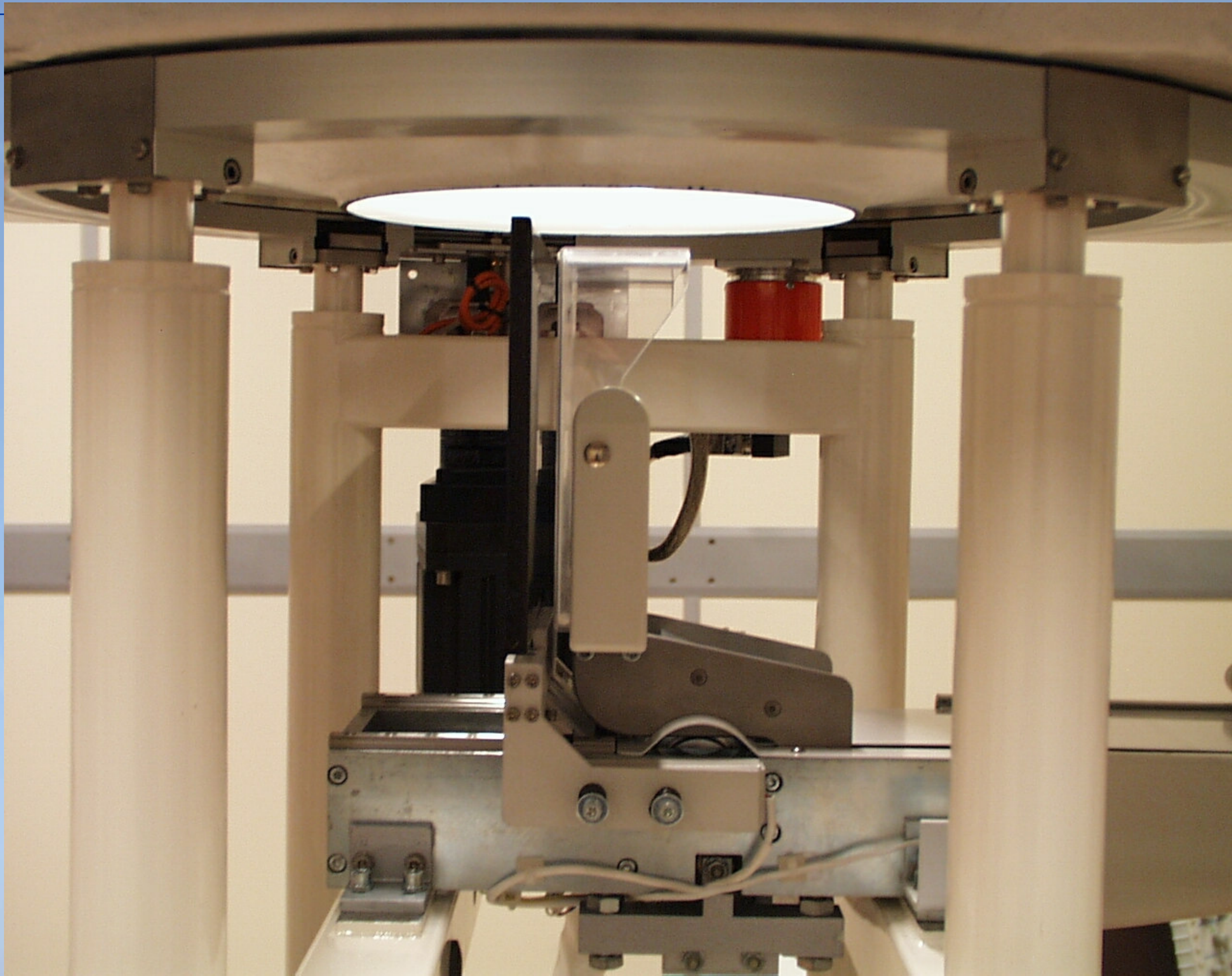

Detector holder

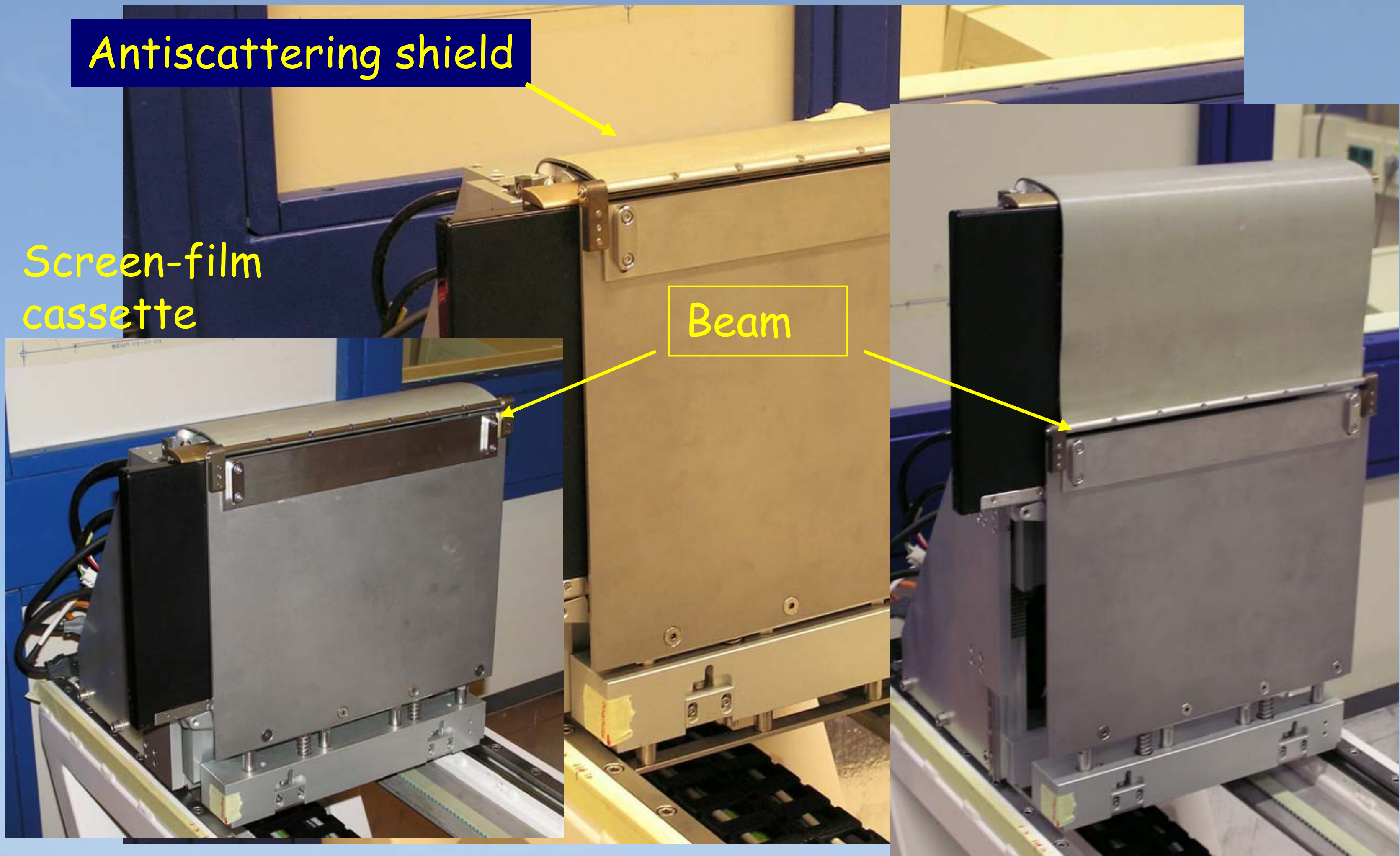

Exposimeters

Based on 4 high-performance diodes

- ✓ excellent charge collection efficiency due to high-purity processing
- ✓ stable operation in harsh radiation environment
- ✓ low light sensitivity

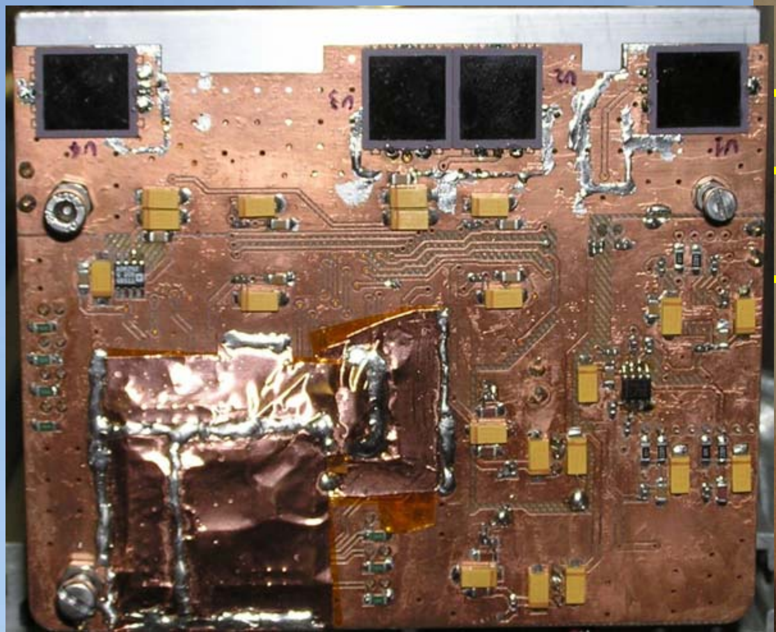

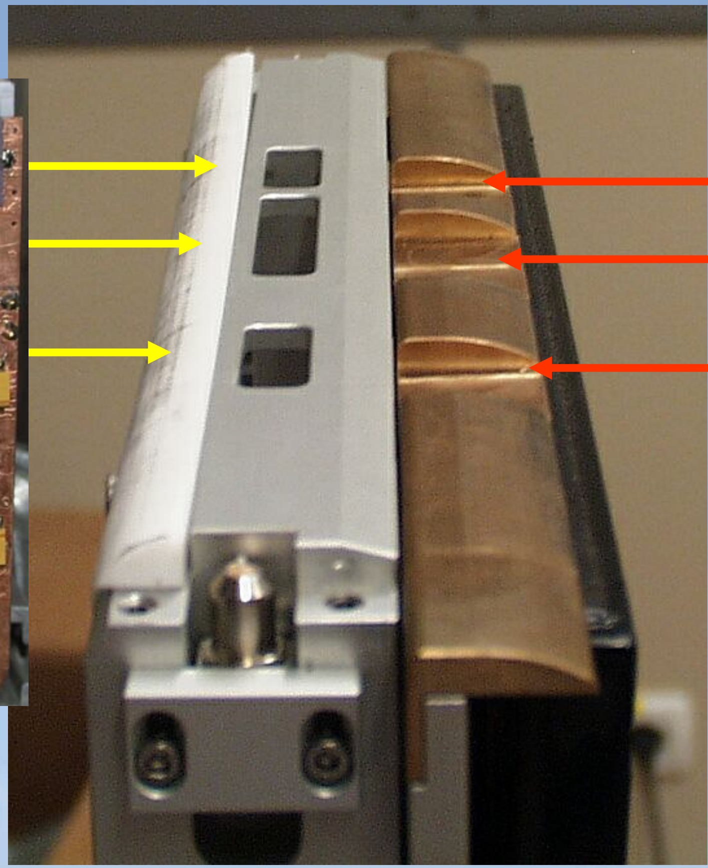

- On board read-out electronics
- Digital output by means of optical fiber

Examination protocol: pre-exposure

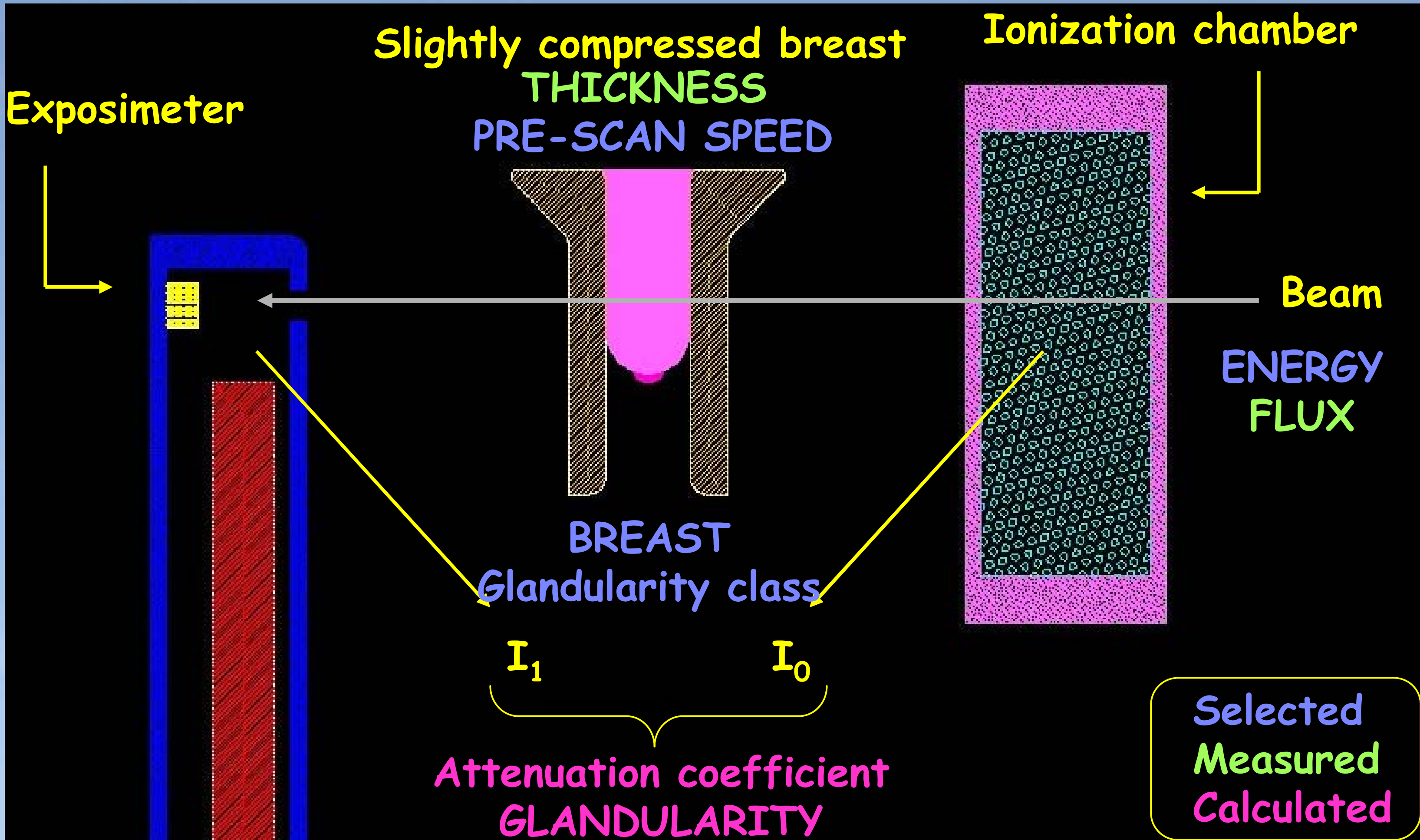

Film is removed from the beam

Examination protocol: exposure

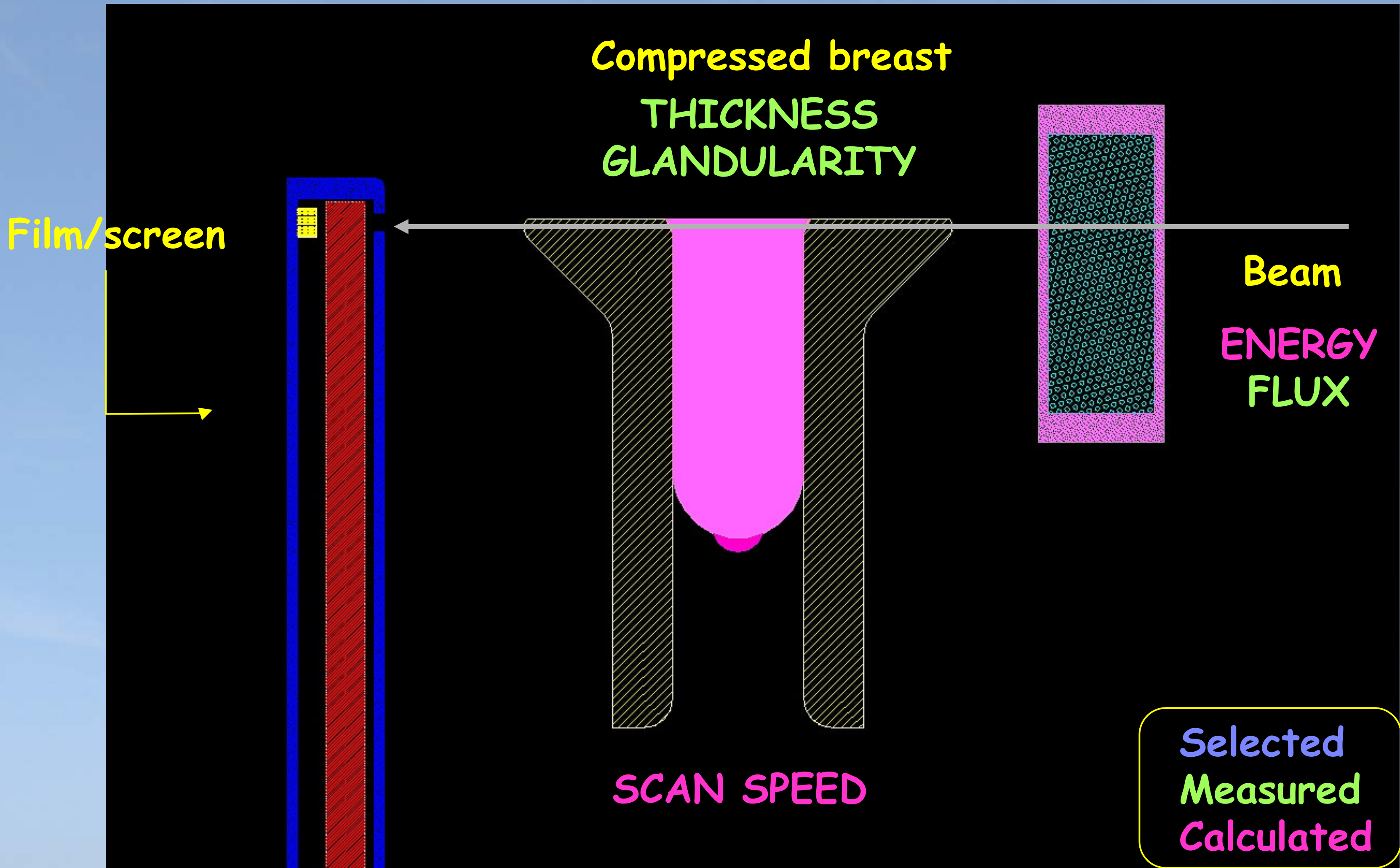


E=18 keV,
MGD$_{st}$=1.1 mGy


E=20 keV,
MGD$_{st}$=0.49 mGy


E=22 keV,
MGD$_{st}$=0.26 mGy

Pat. 8 - 164839 – GA

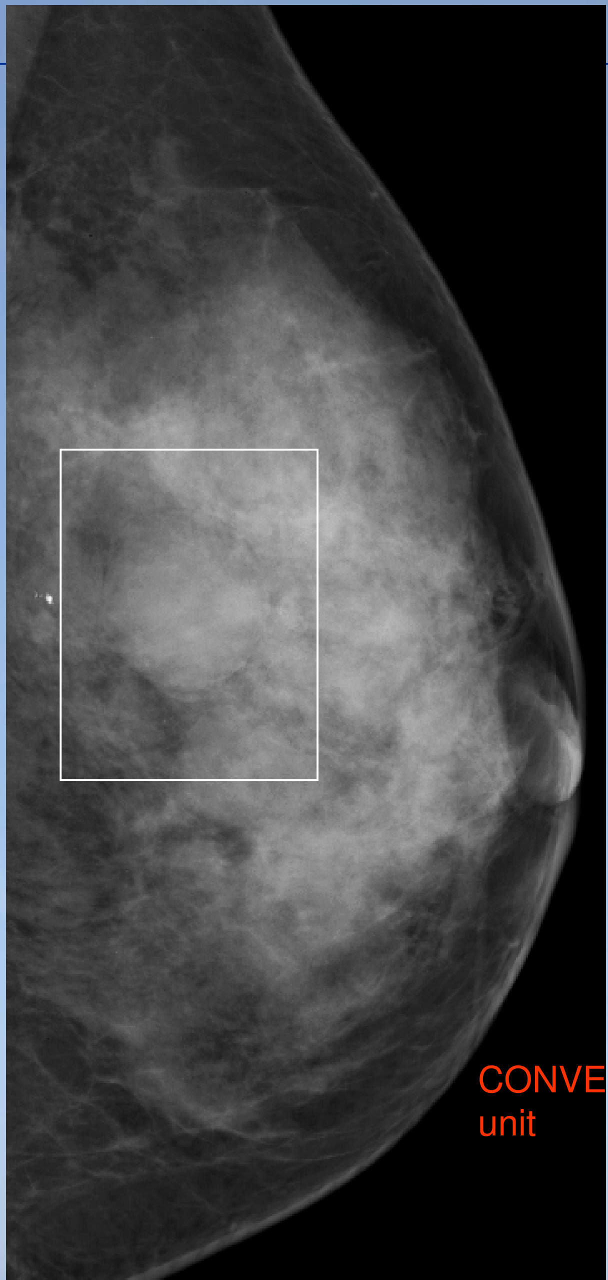

CONVENTIONAL
unit

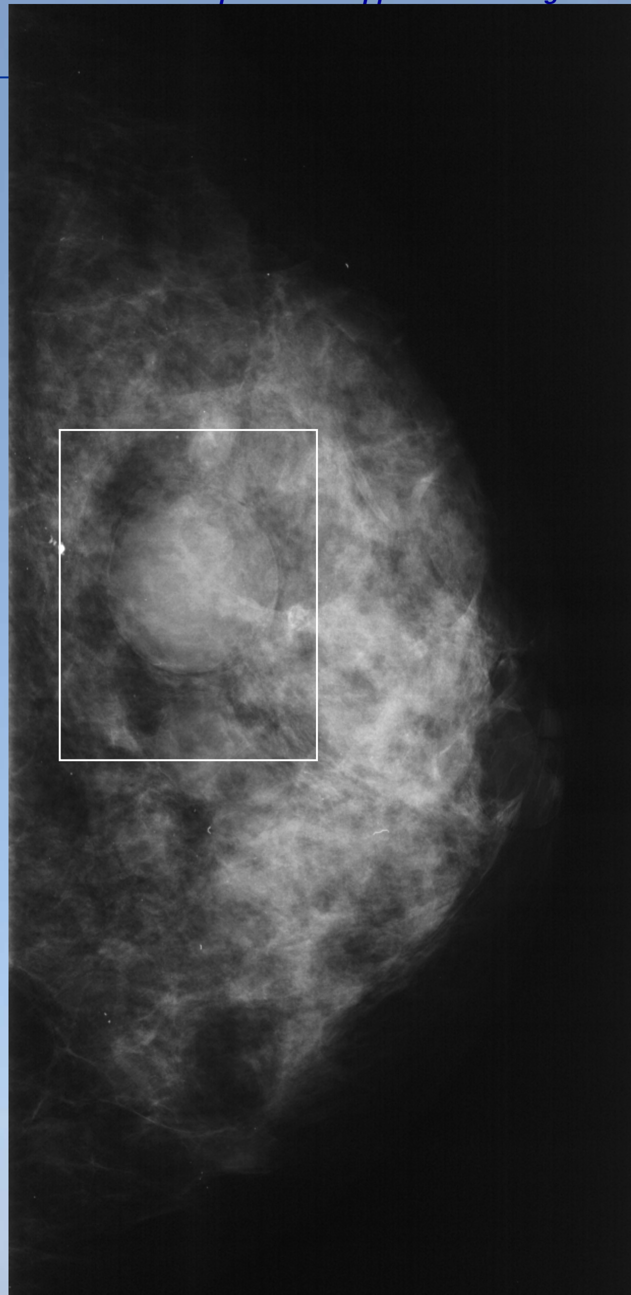

Synchrotron
Radiation

Pat. 8 - 164839 – GA – zoomed view of box region

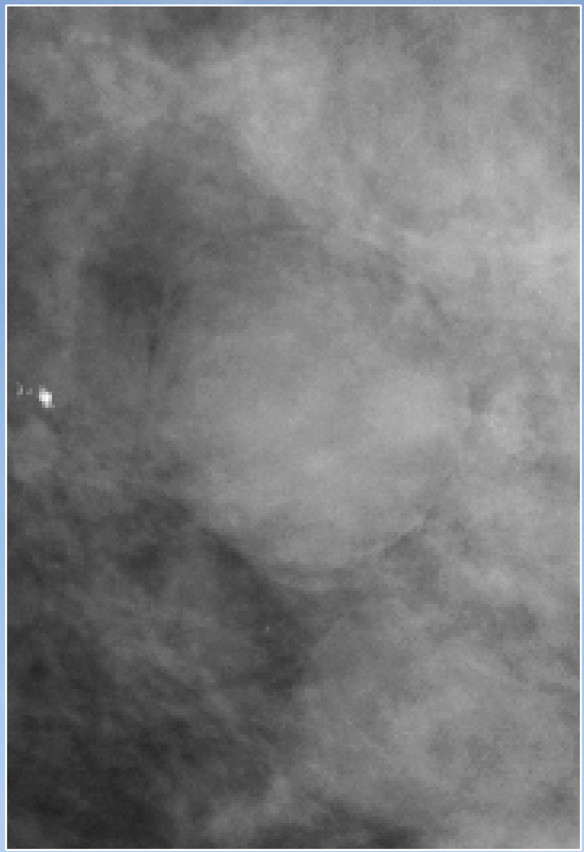

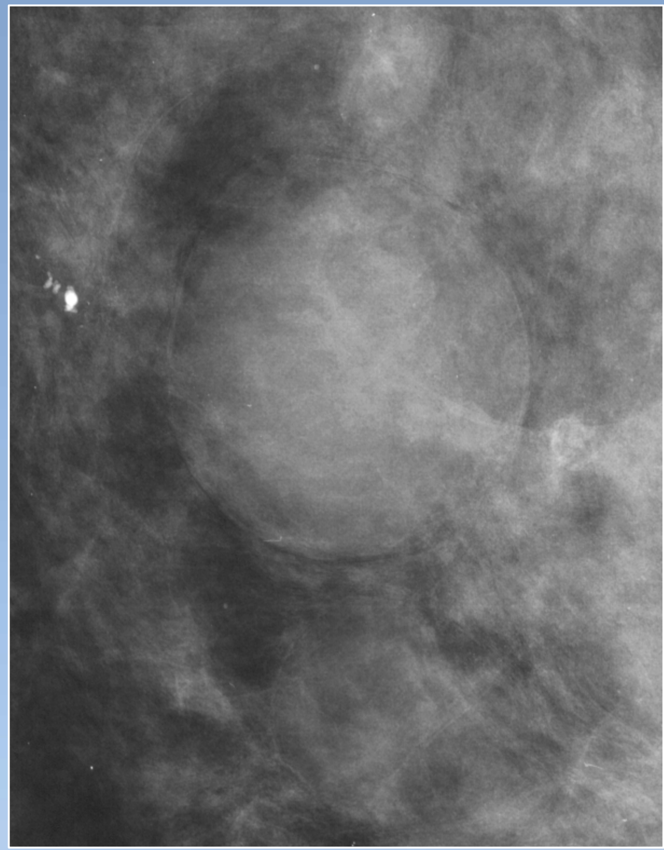

Conventional unit

Synchrotron radiation

Doses comparison

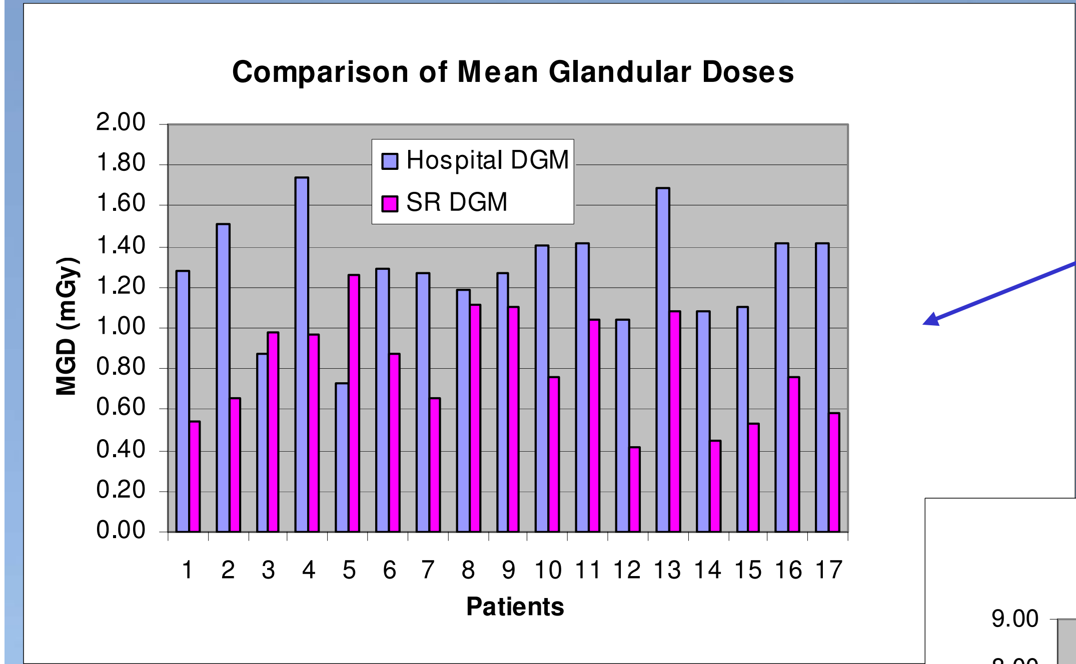

MGD

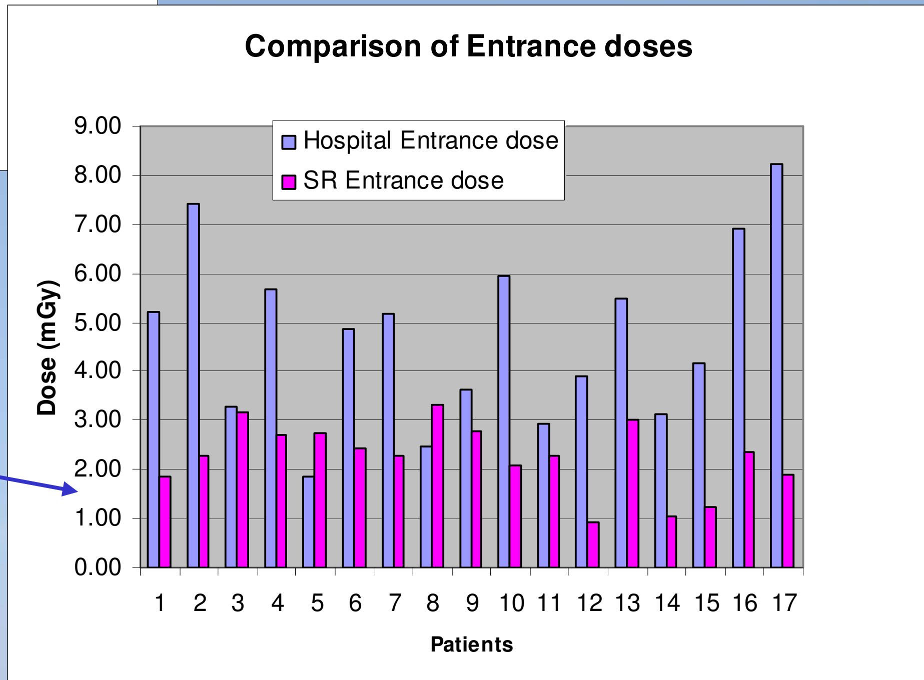

Entrance dose

Imaging of a Brain Tumor using SR

Glioblastoma multiforme (GBM) is the most common and most aggressive primary brain tumor in humans.

One reason for the high rate of recurrence is the invasive nature of the tumor into the surrounding normal brain tissue or multifocal occurrence at sites remote from that of the primary tumor. An imaging protocol that will allow to make visible the invasive nature of the tumor as well as metastases has been developed.

An animal model is used to study malignant brain tumor. C6 glioma cells were cultured and some of the cultures were exposed to colloidal gold for 22 hrs before harvest.

C6 glioma cells were implanted into the brain of adult male Wistar rats. The implantation was performed with the animals under general anesthesia. The animals were allowed to recover after the end of the implantation and were sacrificed two weeks after the tumor cell implantation. We then employed SR PHC technique to image the tumor.

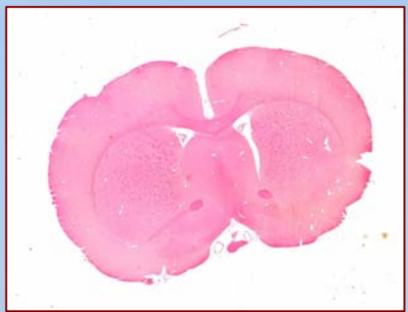

Section of healthy rat brain

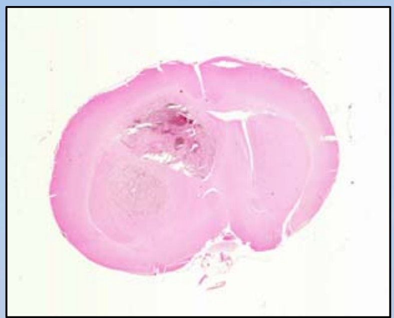

Section of rat brain with C6 glioma 2 weeks after implantation

C.Hall, E. Schultke et al.

E = 24 keV
Sample-to-detector dist. = 80 cm
Num. projections = 720
Ccd pixel size = 14µm

3D rendering of a 4 mm thick volume.

<u>Legenda:</u>

A 1 and A 2:
Tumor without colloidal gold

B 1 and B 2:
Tumor developed after implantation of 300,000 gold-loaded cells

NOTE:
In the skull segments (A2 and B2), the hole created for cell implantation is well visible (diameter 0.6 mm).

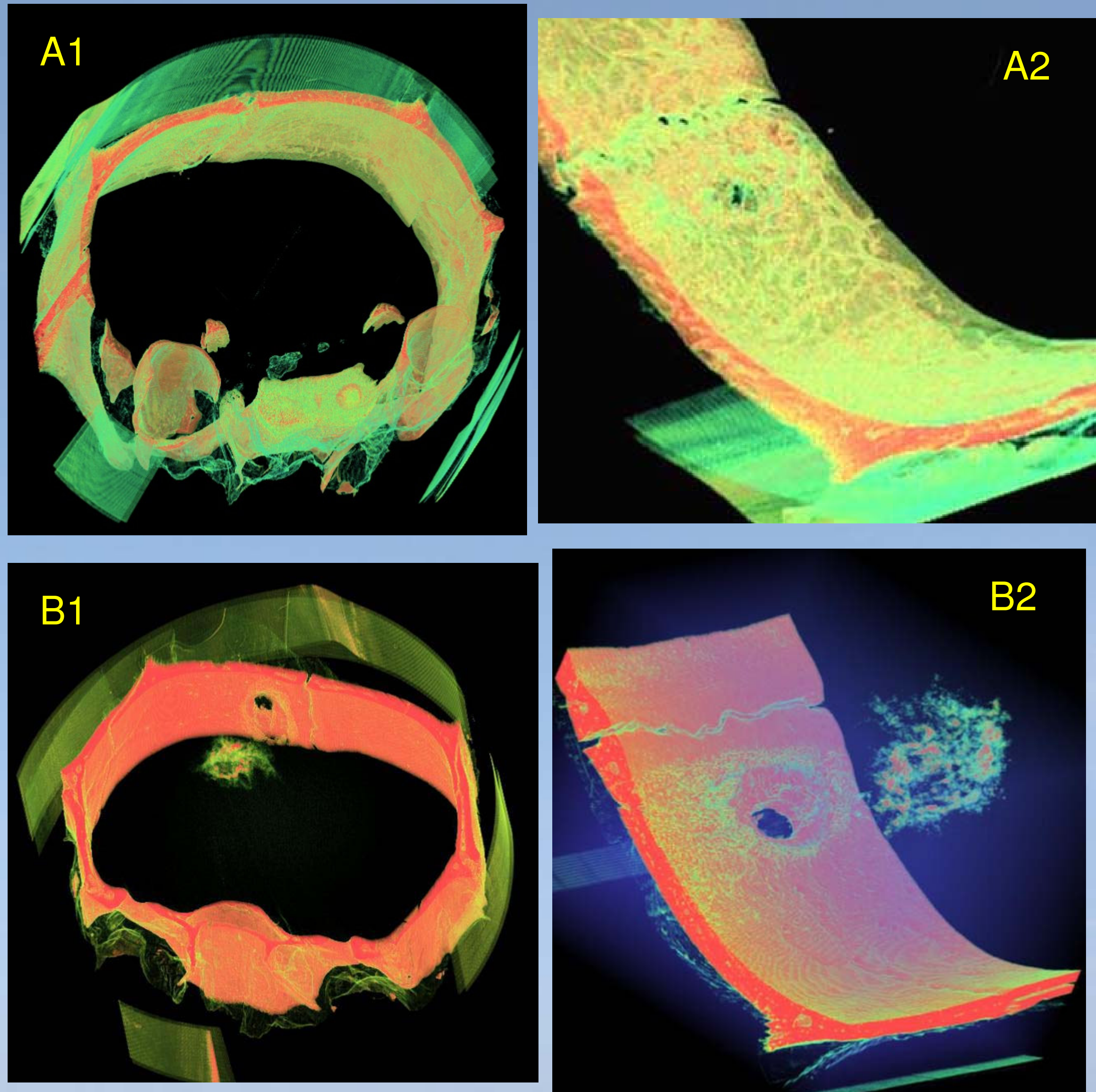

C.Hall, E. Schultke et al.

Lungs imaging with DEI

The potential of DEI technique is under evaluation in different contexts :

- cancer detection
- asthma
- pulmonary emphysema

Problems

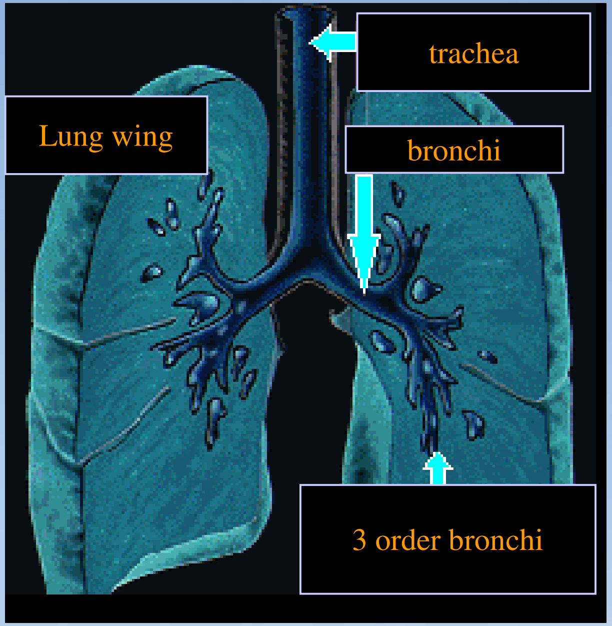

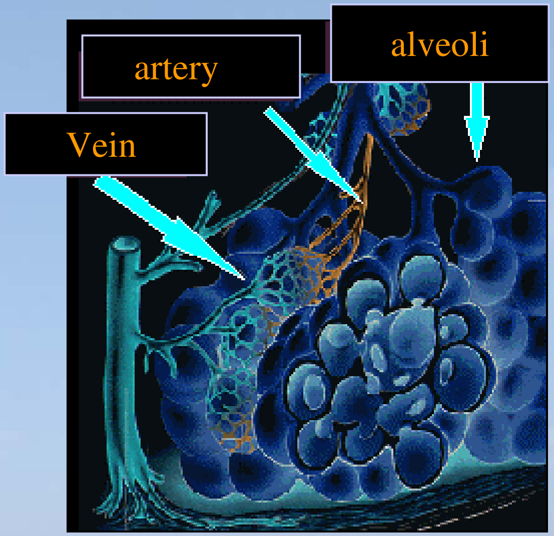

Mouse lungs

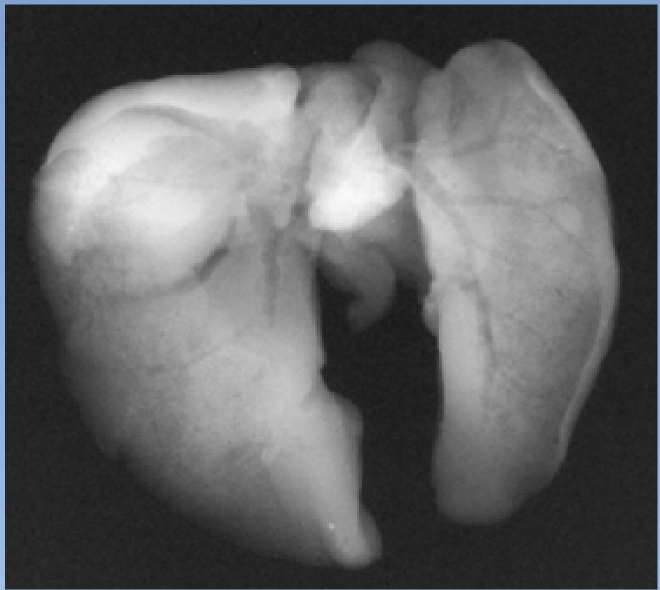

Transmission image

Apparent absorption image

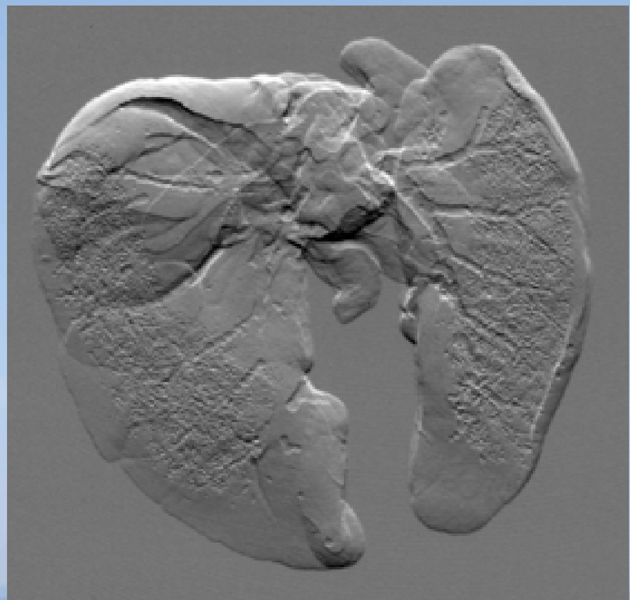

Refraction image

Images at 17 keV

Daresbury, Elettra, University of Trieste Collaboration within PHASY project: R. Lewis, C. Hall, et Al.

Mouse lungs

Top image

Images at 17 keV

Far slope image

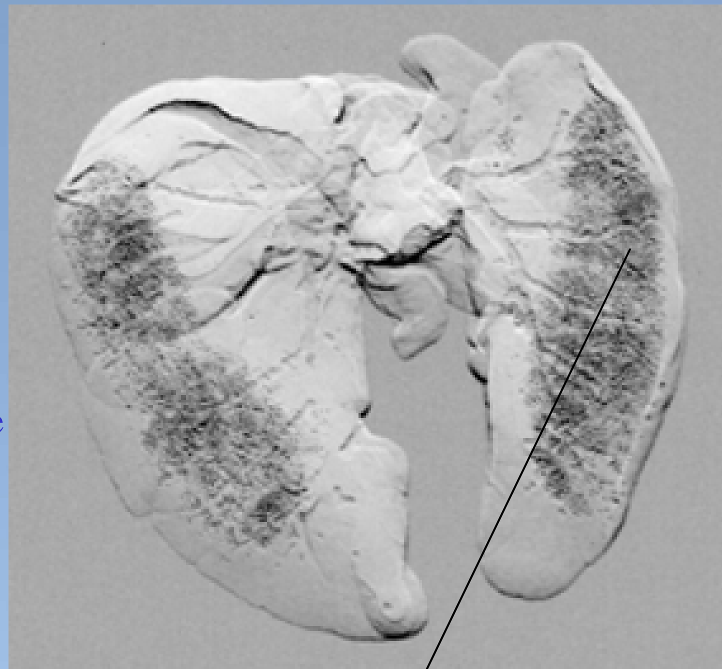

Zoom of top
extinction contrast

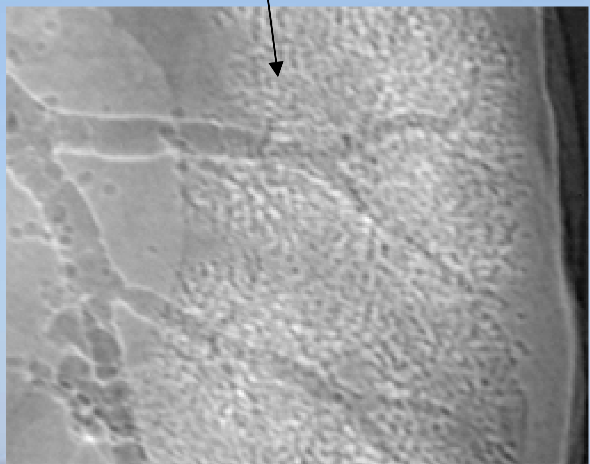

Zoom of far slope
reverse contrast

Finger Joint

Conventional radiograph

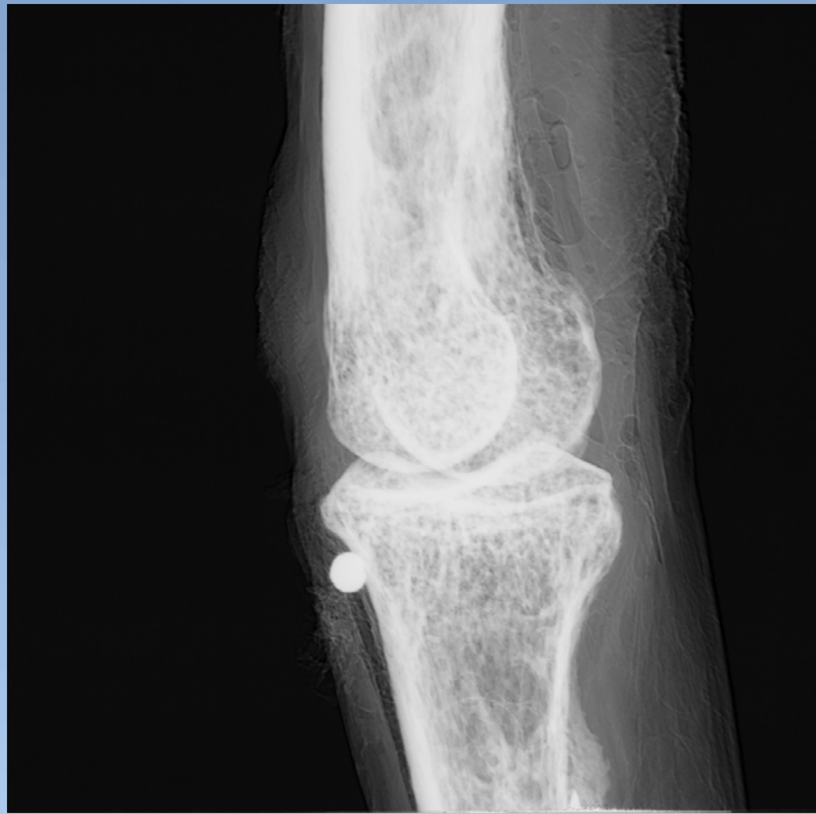

Apparent absorption image @ 20 keV
at ELETTRA

Daresbury, Elettra, University of Trieste Collaboration within PHASY project: R. Lewis et al.

Index finger proximal interphalangeal joint

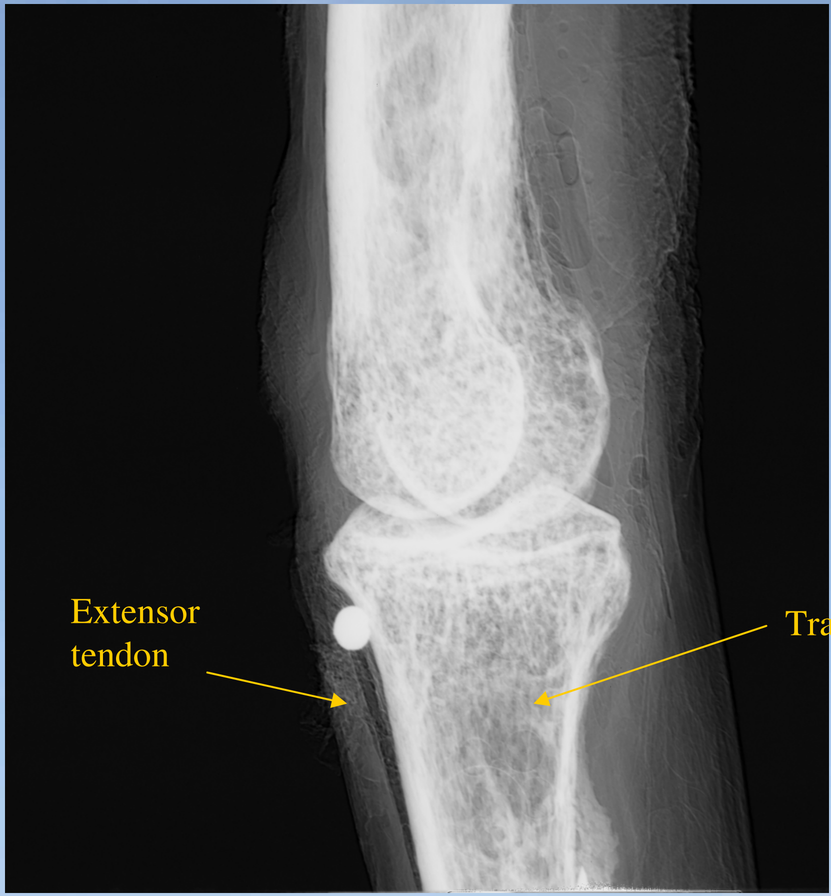

Apparent absorption Image

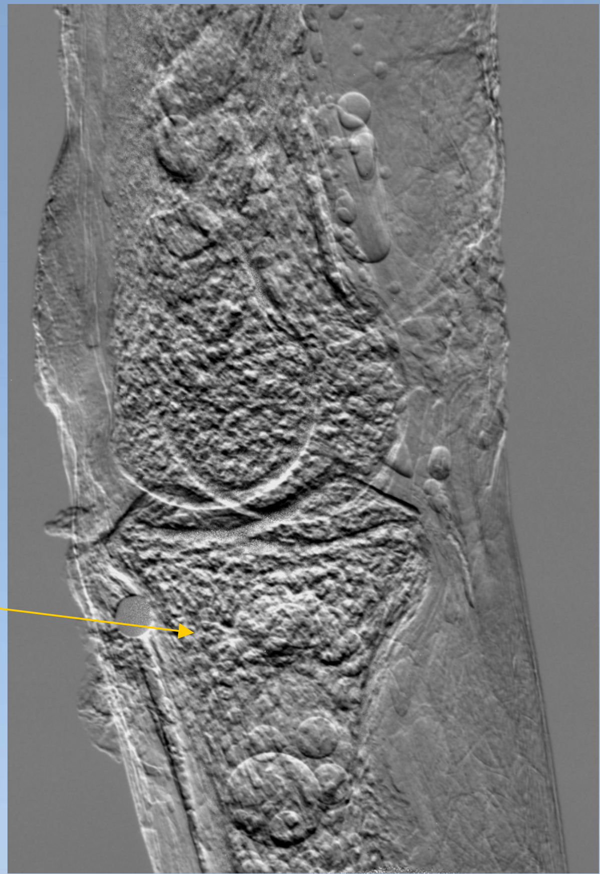

Refraction Image

Index finger proximal interphalangeal joint

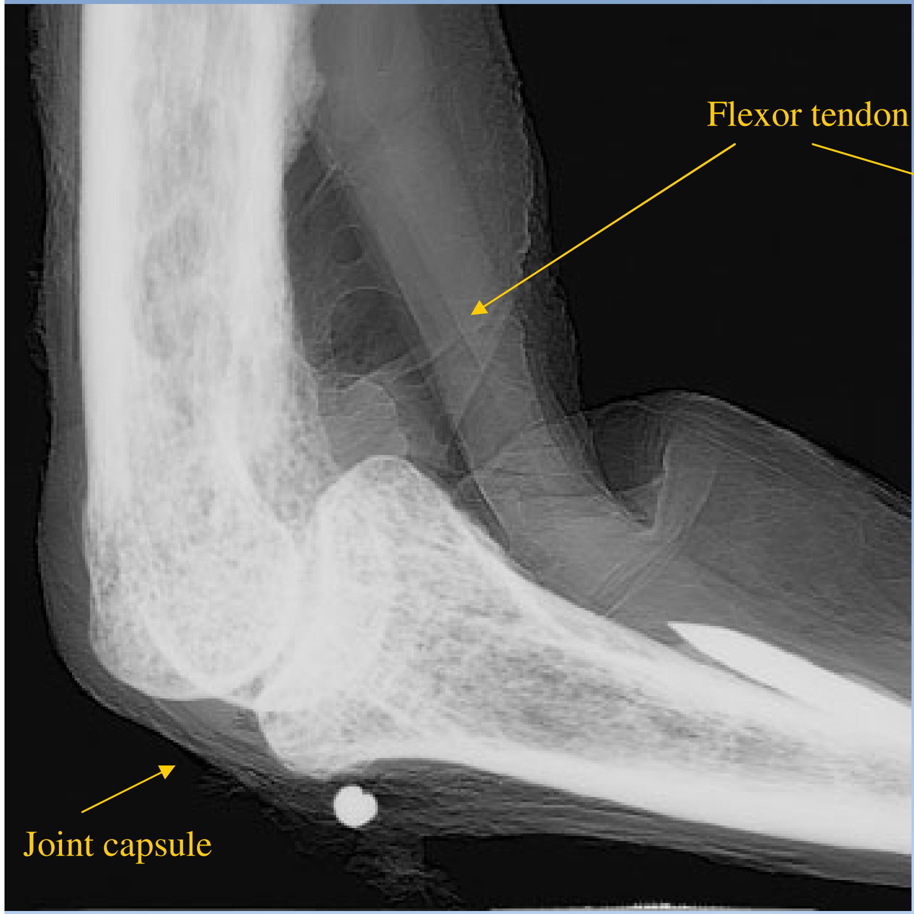

Apparent absorption Image

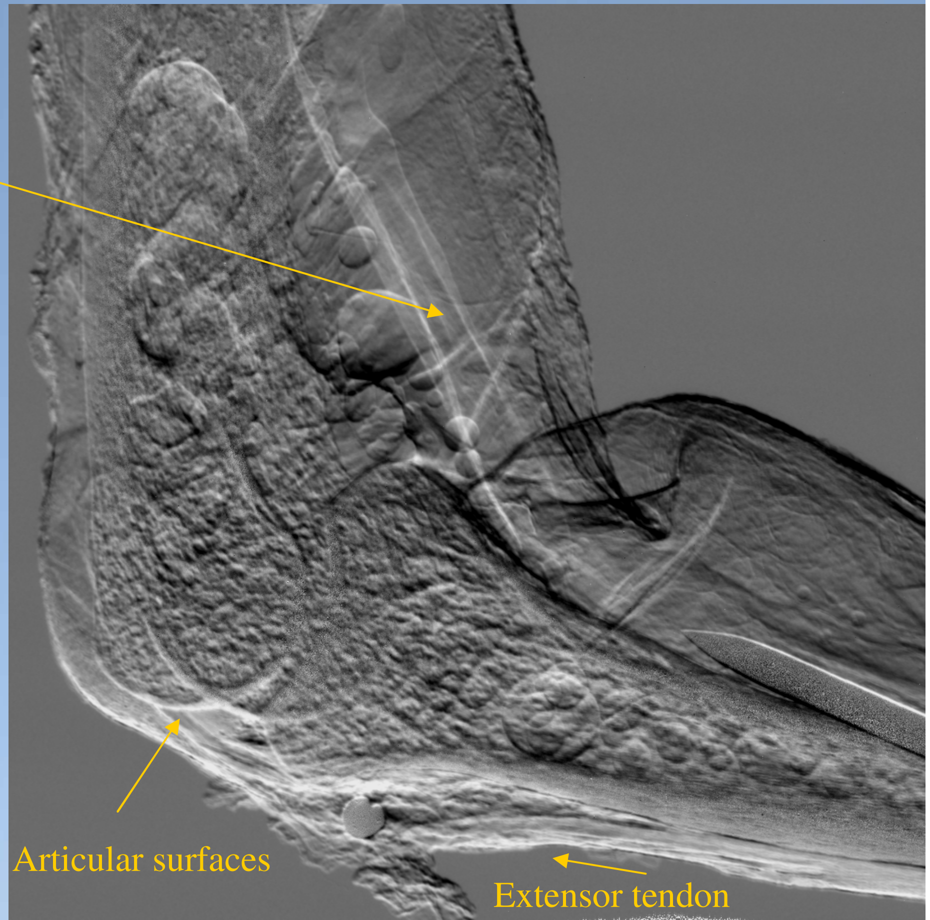

Refraction Image

Computed μ-Tomography (μ - CT)

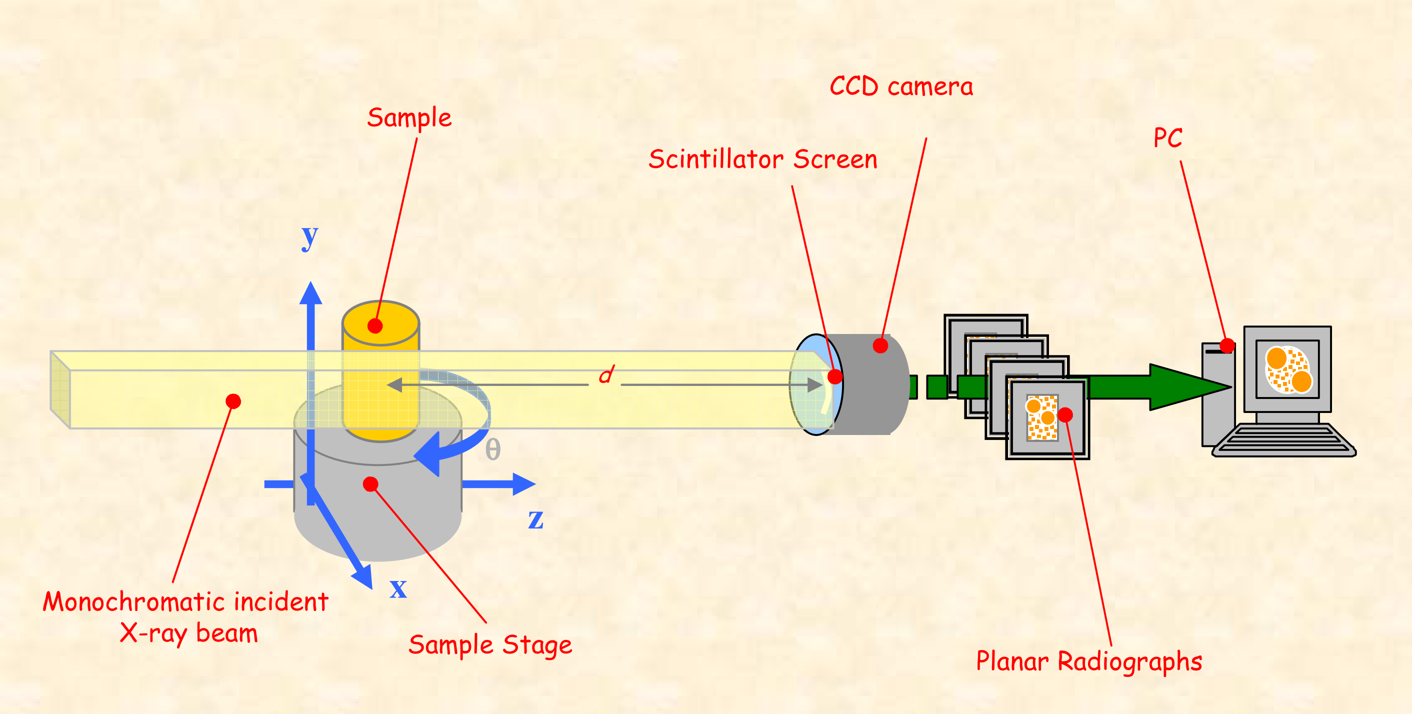

- μ -CT allows to investigate the **internal features** of a sample **without sectioning** it:
  - → in many cases the **sectioning procedure** modifies the sample structure
  - → the sample can be after **studied by other** experimental **techniques**,
  - → or submitted to several **treatments** (mechanical, thermal, etc...)

Study of trabecular bone structure

- In the adult there are two main kinds of bones: the cancellous (trabecular) and the compact one. The first is mainly involved in the metabolic processes of calcium homeostasis while the second has principally the mechanical function of support.
- Osteoporosis causes alterations in the trabecular bone that produce a reduction of bone mass but also by structural changes in the bone architecture.
- Bone mineral density is often estimated *in vivo* using Dual Energy X-ray Absorptiometry which evaluates the mineral contenent of bone.
- The quantification of bone microarchitecture is mainly based on histology that allows to extract histomorphometric parameters quantifying bone structure in terms of shape, connectivity etc.. <u>This techique is destructive</u>.

Absorption μ - CT: Trabecular bone structure

Elastic properties of bones are determined by: composition, density and bone architecture.

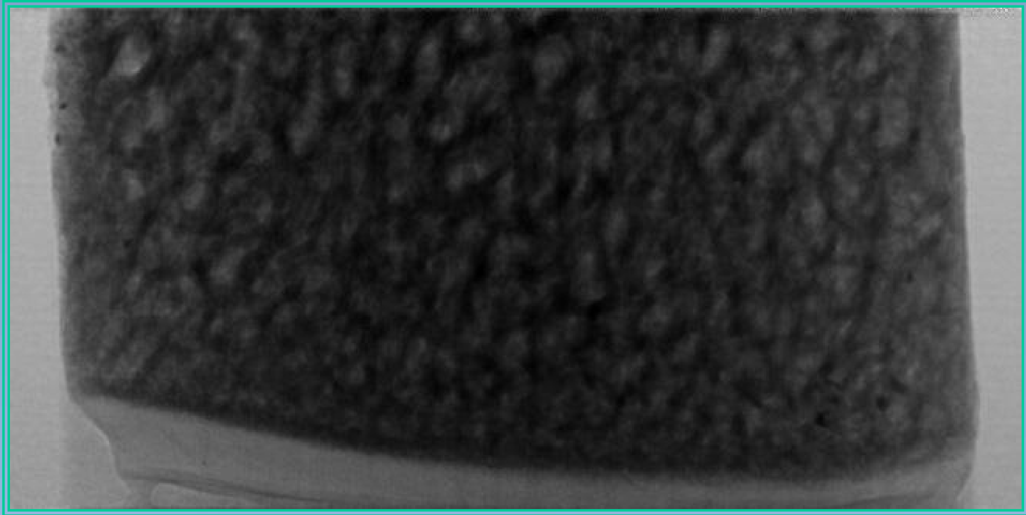

E= 26 keV
Absorption radiograph

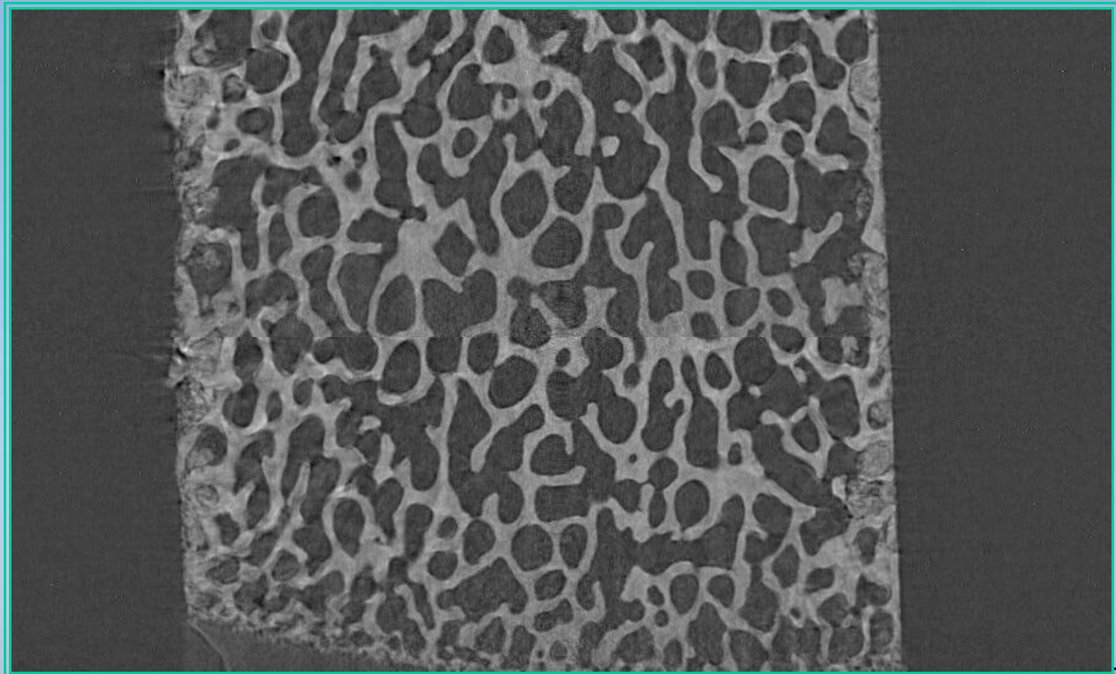

E= 26 keV
Absorption tomograph

Samples by: D.Dreossi, F.Vittur, F.Cosmi
University of Trieste

Reconstructed volume from a sample of pig trabecular bone

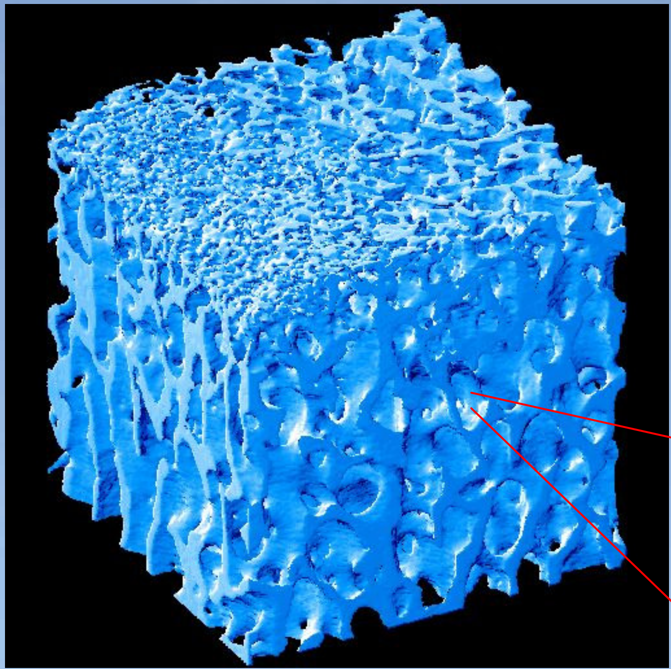

224 pixels voxel

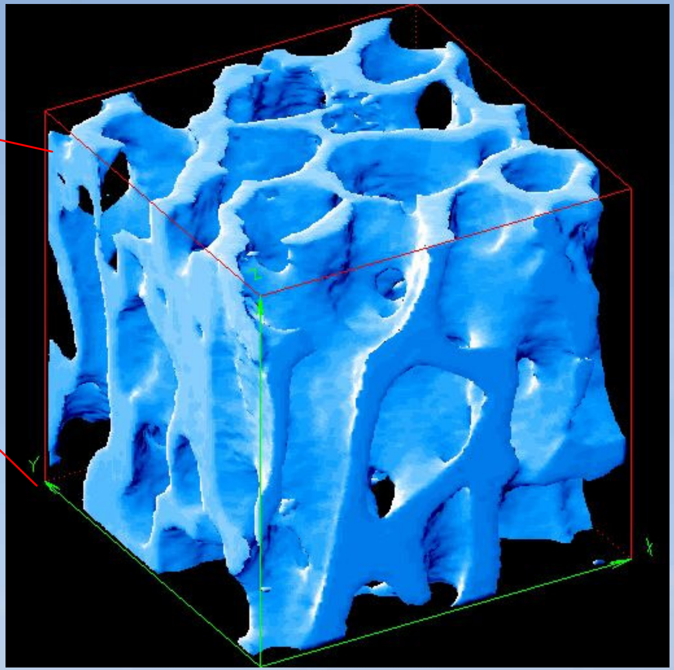

100 pixels voxel

High resolution μ-CT analysis of a proximal human femur with an innovative linear detector

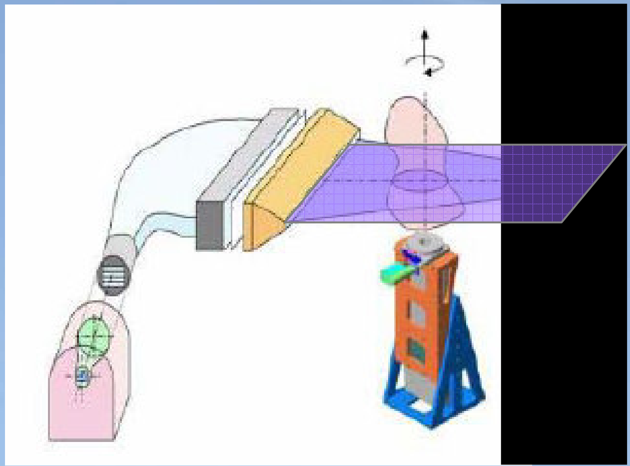

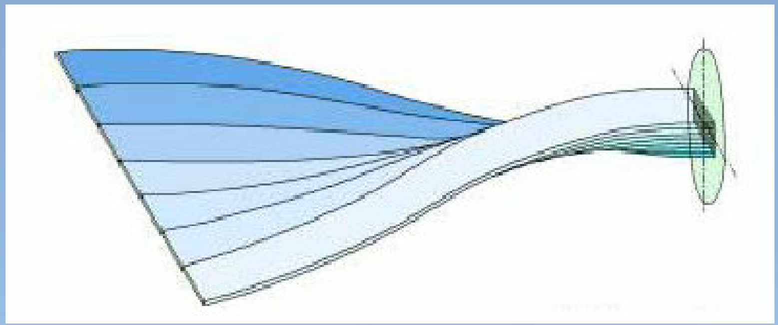

- Investigation of the **performance of a EBCCD-based system** with a nominal spatial resolution of 22.5 μm extended over a **FOV of 130 mm x 1 mm**.
- This system is obtained by using **a distinctive fiberoptic ribbon** (patented by the **University of Bologna**) converting a linear geometry to a rectangular one.
- A scan of **a 9 cm wide human proximal femur** allowed to analyze the trabecular structure of the bone in order to investigate changes caused by **osteoporosis**.

A. Pasini et al., Proceedings of IEEE NSS/MIC 2004 Annual meeting, Rome, Italy

ISTITUTI ORTOPEDICI RIZZOLI

10 cm

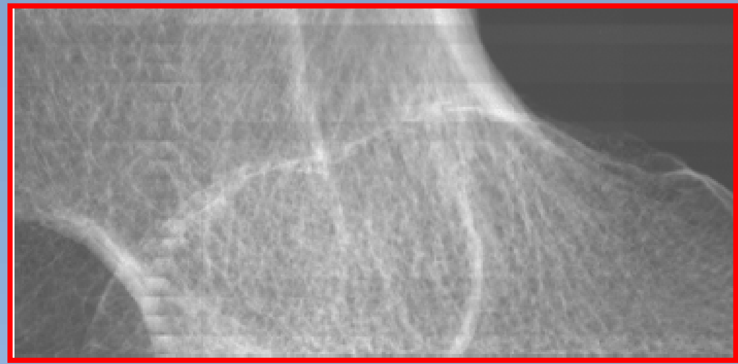

t_{exp} = 600 sec

E = 34 keV

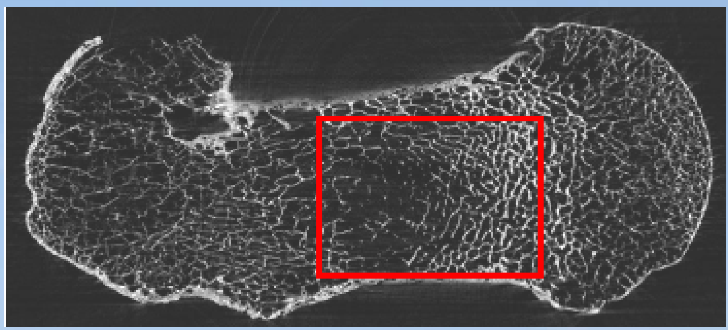

Reconstructed slice

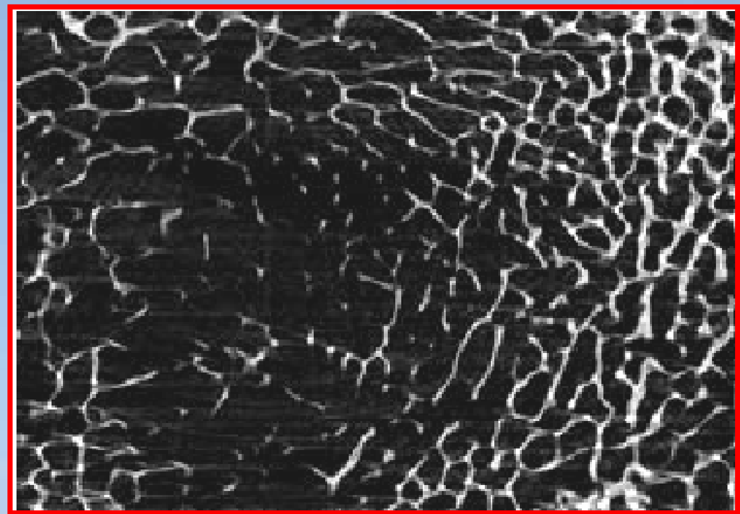

A. Pasini et al., Proceedings of IEEE NSS/MIC 2004 Annual meeting, Rome, Italy

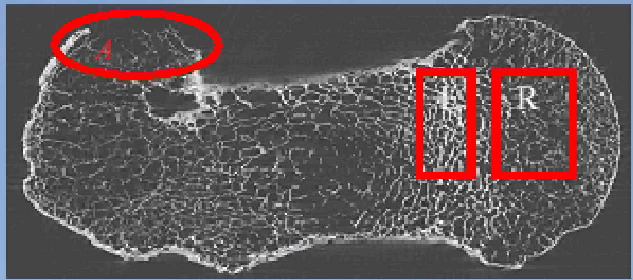

	BV/TV [%]	Tb.Th [μm]	Tb.N [mm^{-1}]	Tb.Sp [μm]
Left ROI	21.4±0.3	167±2	1.28±0.03	610±20
Right ROI	13.8±0.2	120±1	1.17±0.02	740±10

	BV/TV [%]	Tb.Th [μm]	Tb.N [mm^{-1}]	Tb.Sp [μm]
Big ROI	17.5±0.2	122±2	1.44±0.02	576±8

LEGENDA:
BV/TV – Bone Volume/Tissue Volume
Tb.Th – Trabecular thickness
Tb.N – Trabecular Number
Tb.Sp – Trabecular Space

Rendering of 50 slices

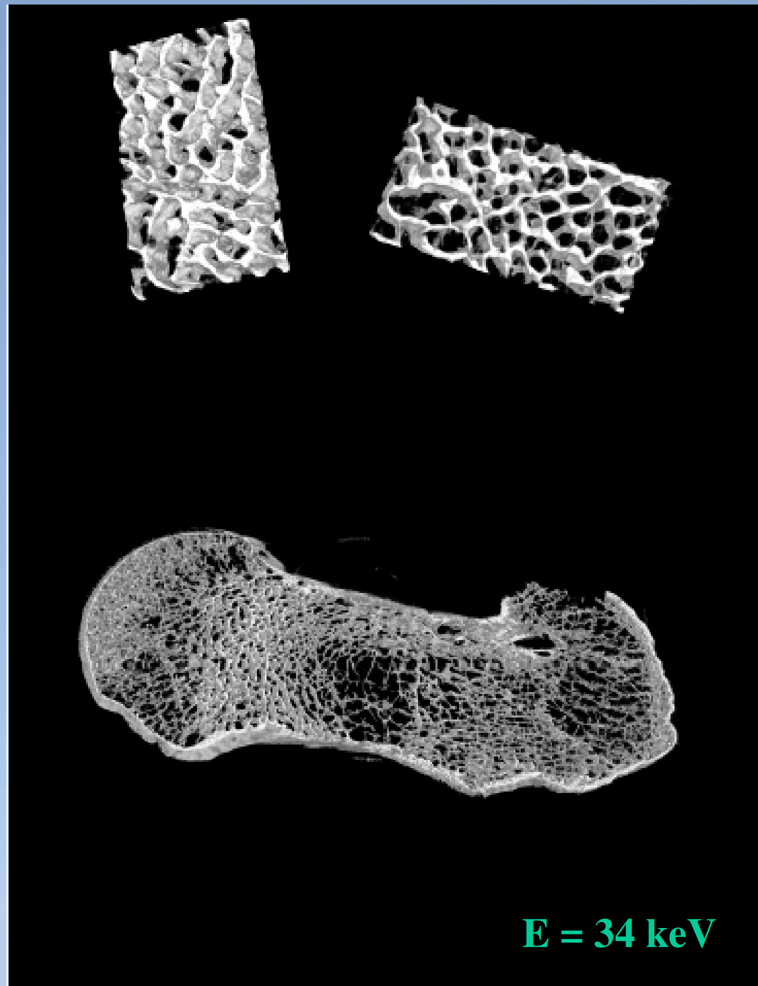

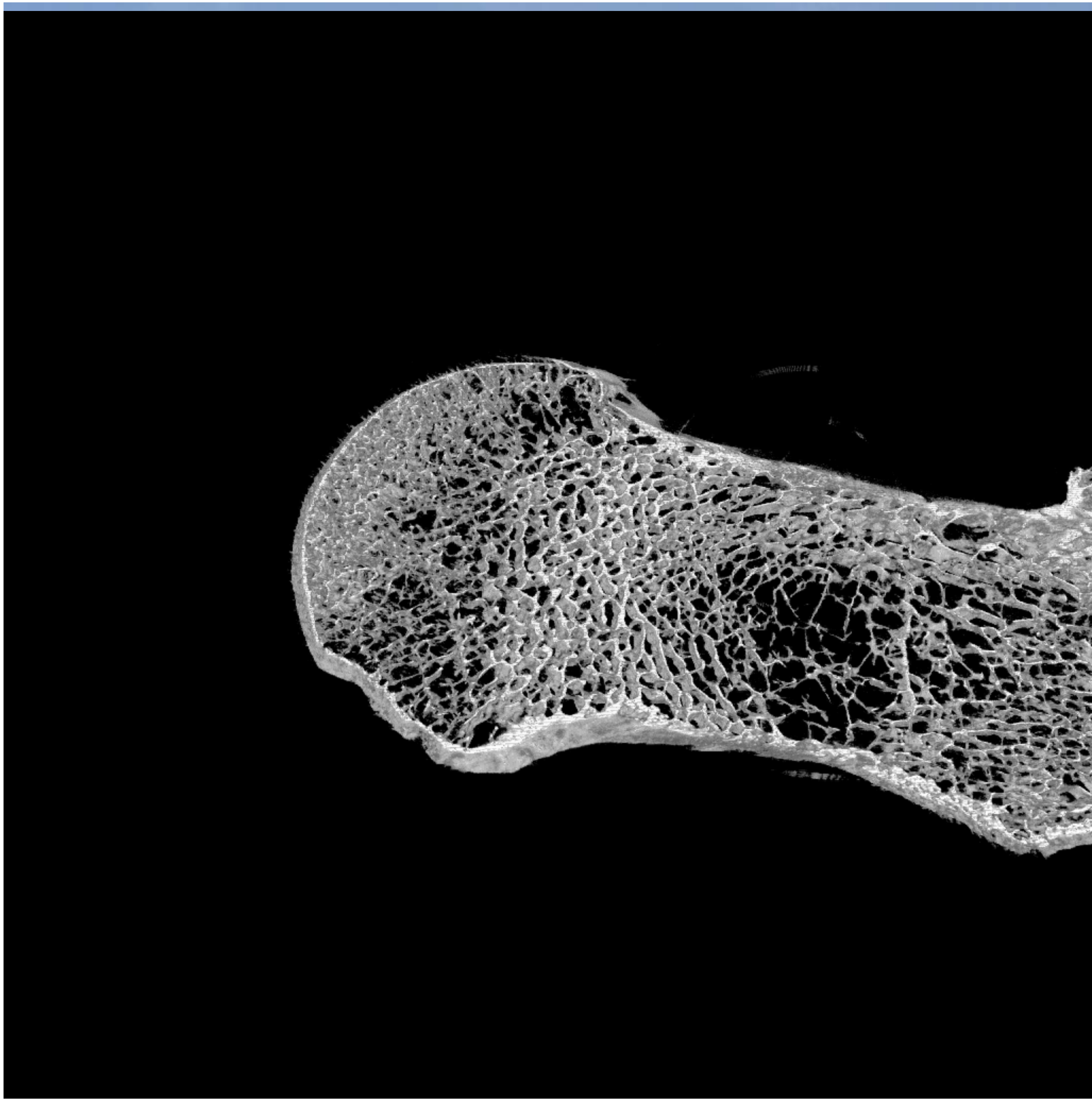

3D volume rendering

50 slices

Study of the bone structure adjacent to oral implants

- One of the most important aims about **cortical and cancellous bone** researches is to understand the factors that determine their **mechanical properties**, how these properties are maintained, and how bone reacts to changes in its environment, such as the introduction of a **Ti implant**.
- **Trabecular morphometry** has been traditionally assessed in **2D**. Particularly limiting is the **destructive** nature of this extremely time consuming procedure. Synchrotron radiation **X-ray microtomography** allows to investigate the **3D microstructure** of bone.
- Beam energies between 30 and 40 keV will provide **a satisfactory signal-to noise ratio** and contrast for the bone, except for the parts falling in the shadow of the Ti screw. Then, we investigated the effect of **Al implants**.

L. Tesei, F. Casseler, D. Dreossi, F. Zanini, L. Mancini, G. Tromba

Reconstructed slice obtained at the ESRF

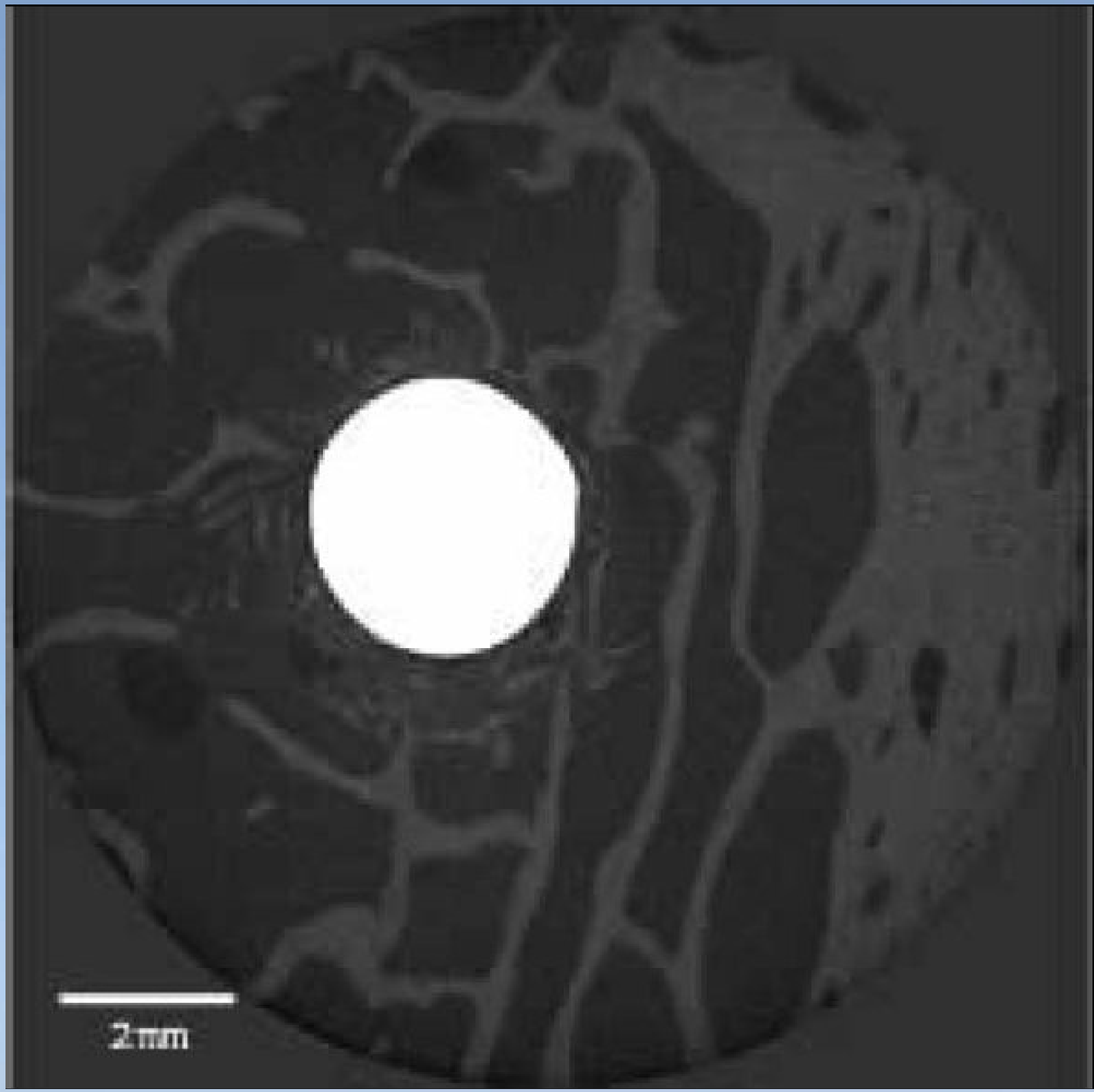

E = 50 keV

L. Tesei et al., NIM A, 548 (2005) 257-263

Comparison before and after the bone implant

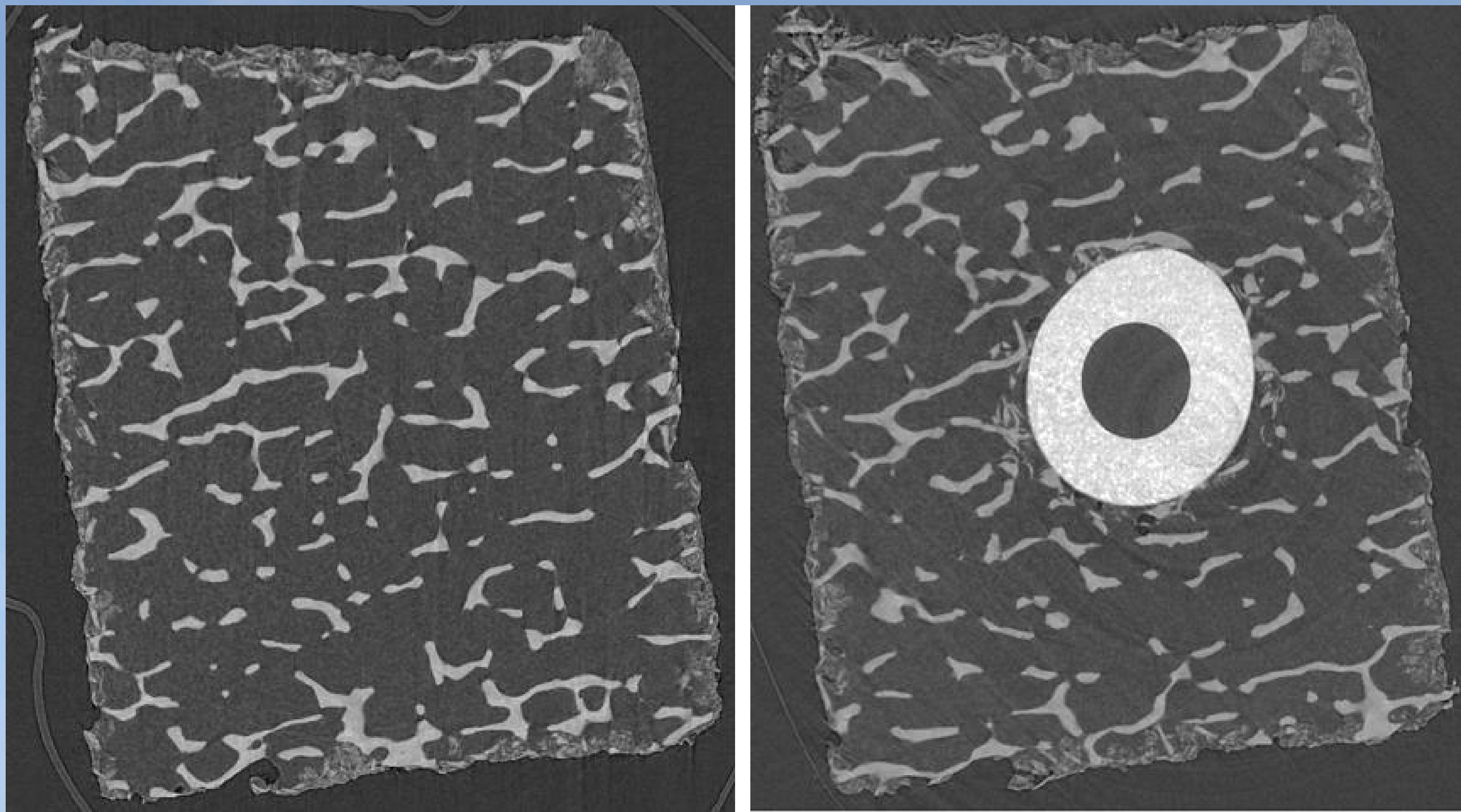

2 mm

E = 29 keV, ***d*** **= 17 cm**

L. Tesei et al., NIM A, 548 (2005) 257-263

Study of the bone damage around the implant

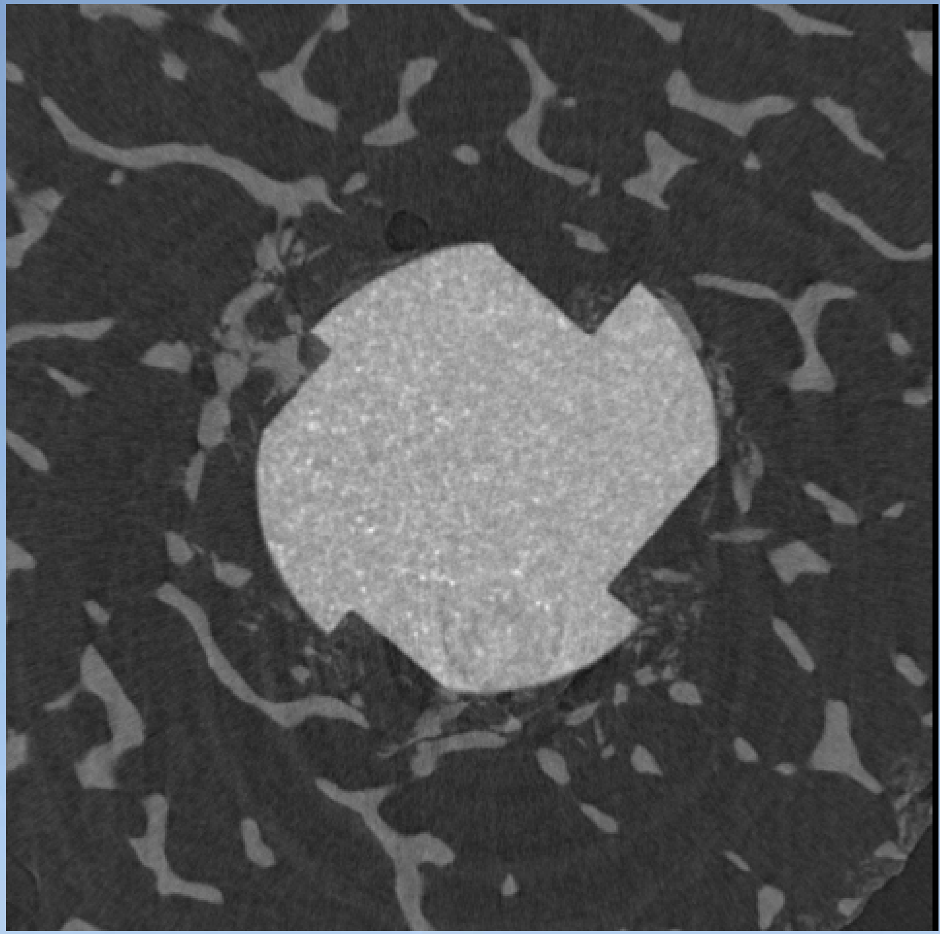

Screw: ∅ 3mm, anchorage length 8.5 mm

1 mm

E = 29 keV, *d* = 17 cm

L. Tesei et al., NIM A, 548 (2005) 257-263

3D rendering of the implanted bone

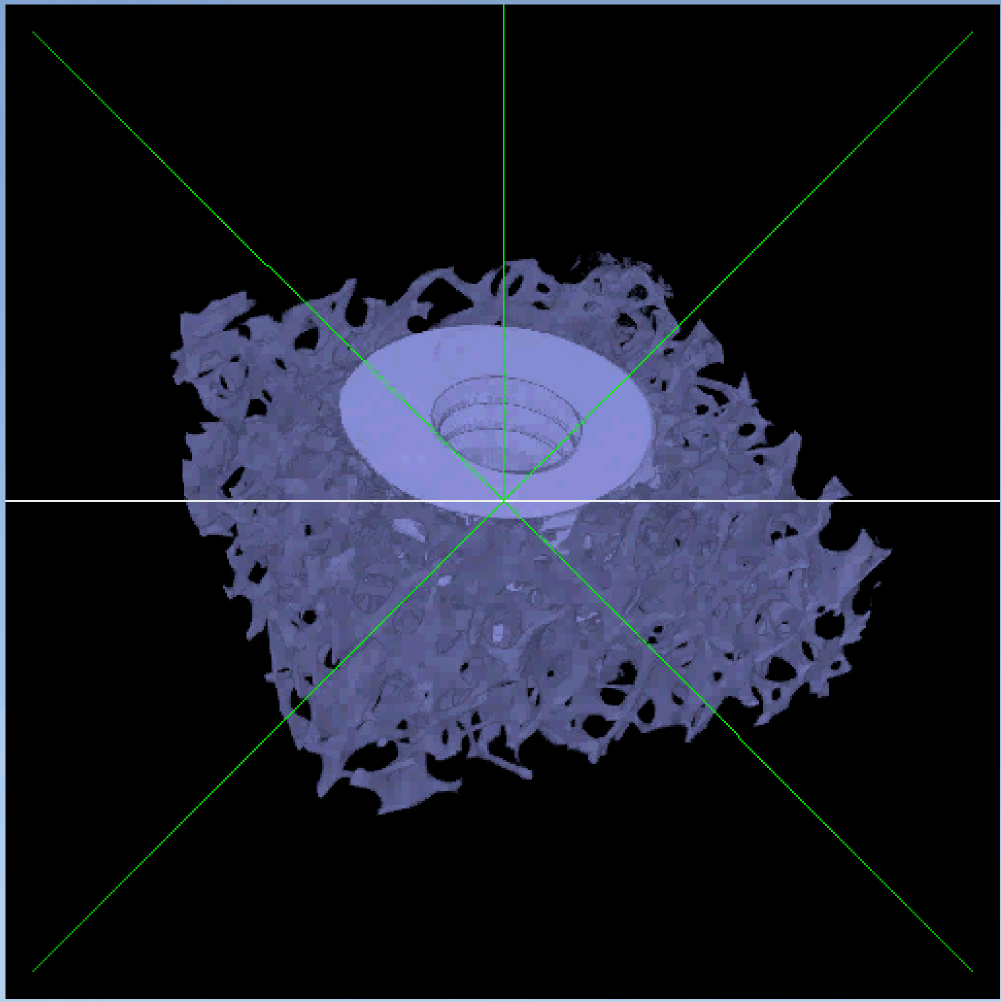

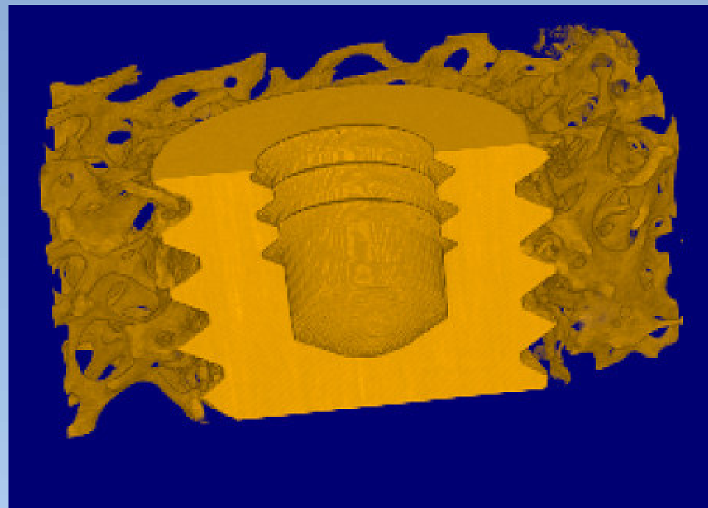

1 mm

E = 29 keV, *d* = 17 cm

L. Tesei et al., NIM A, 548 (2005) 257-263

Acknowledgements

to the SYRMA/SYRMEP team:

A.Abrami, K.Casarin, V.Chenda, C.Fava, L.Mancini, R.H. Menk, E.Quai, A.Vascotto, F.Zanini
Sincrotrone Trieste
L.Rigon
Sincrotrone Trieste and International Center for Theoretical Physics, Trieste
F.Arfelli, E.Castelli, D.Dreossi, R.Longo
Department of Physics - University of Trieste and INFN
M.A. Cova, M. Tonutti, F. Zanconati
Department of Radiology - University and Hospital, Trieste
F. de Guarrini, P. Bregant
Health Physics - Hospital, Trieste

and to external collaborators:
F.Casali et al.: University of Bologna
C.Hall et al.: Daresbury laboratory
S. Majumdar et al, University of California
R.Lewis et al.,Monash University, Melburne
L.Tesei, I. Teseo Tesei Trieste
…….